

**UNCLASSIFIED**

**AD 409 624**

---

**DEFENSE DOCUMENTATION CENTER**

**FOR**

**SCIENTIFIC AND TECHNICAL INFORMATION**

**CAMERON STATION, ALEXANDRIA, VIRGINIA**



**UNCLASSIFIED**

NOTICE: When government or other drawings, specifications or other data are used for any purpose other than in connection with a definitely related government procurement operation, the U. S. Government thereby incurs no responsibility, nor any obligation whatsoever; and the fact that the Government may have formulated, furnished, or in any way supplied the said drawings, specifications, or other data is not to be regarded by implication or otherwise as in any manner licensing the holder or any other person or corporation, or conveying any rights or permission to manufacture, use or sell any patented invention that may in any way be related thereto.

AFUSK 4755

63-4-2

CoA NOTE 135

CATALOGED BY DDC  
AS AD No. 409624

409 624

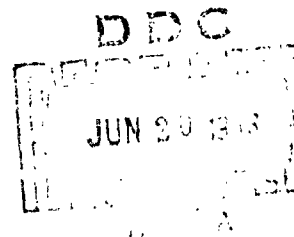


THE COLLEGE OF AERONAUTICS  
CRANFIELD

STUDY OF HEAT AND MASS TRANSFER  
FROM NON-ISOTHERMAL SURFACES

by

A. G. Smith and V. L. Shah



AFUSK 4755

COLLEGE OF AERONAUTICS NOTE NO.135

ASTIA DOCUMENT NO: AD

CONTRACT AF 61(052)-267

TECHNICAL REPORT

THEORETICAL AND EXPERIMENTAL STUDY OF HEAT  
AND MASS TRANSFER FROM NON-ISOTHERMAL SURFACES

by

A. G. Smith and V. L. Shah

Department of Aircraft Propulsion  
College of Aeronautics  
Cranfield, England

November 1962

"The research reported in this document has been sponsored by PROPULSION RESEARCH DIVISION, AFOSR, OAR, UNITED STATES AIR FORCE, monitored by the European Office, Office of Aerospace Research".

### ACKNOWLEDGEMENT

This research was supported by the United States Air Force under Contract No. AF 61(052)-267, and monitored by the Air Force Office of Scientific Research of the Air Research and Development Command.

The authors are grateful to many individuals in the fulfilment of this research. Professor D. B. Spalding of Imperial College, London, suggested the use of his velocity law in the theoretical investigation. Dr. A. J. M. Spencer, of Nottingham University, assisted with the discussion of the methods of numerical solution. The Department of Mathematics at The College of Aeronautics gave permission to use the Digital Computer, and the Deputy Head of the Department of Aircraft Propulsion, Mr. J. R. Palmer, gave extensive help in the programming for the digital computer.

The authors are also grateful to the Workshop Staff of the Department of Aircraft Propulsion for the manufacture of the test rig. Mr. E. R. Norster gave his assistance in the use of the Infra-red Gas Analyser, T. McNeill assisted in the running of the test rig, and V. Kaul assisted with the experimental measurements.

This work was carried out in the Department of Aircraft Propulsion, The College of Aeronautics, Cranfield, England.

### ABSTRACT

The numerical solution of the partial differential equation in the in-compressible turbulent boundary layer has been obtained for step

$\frac{\dot{q}_w''}{\rho u_1 C_p \sqrt{C_f}/2}$  and for Prandtl numbers 0.7, 1 and 7. The Schmidt method of integration was used and the integration was carried out on a Ferranti Pegasus Digital Computer. A method has been developed to apply this numerical solution for obtaining surface and fluid temperature for the case of arbitrary distribution of heat flux at the surface.

Simultaneously, approximate equations for calculating heat transfer over a flat plate with arbitrary heat flux are derived for laminar and turbulent flow.

To verify the theoretical solution, experiments were made in which the concentration profiles of the injected gas (carbon dioxide) at different stations were measured when the pipe had another gas (air) flowing turbulently through in the axial direction, and the gas injected was passed through a porous section of the tube wall.

## CONTENTS

### Acknowledgement

### Abstract

### Contents

1. Introduction
  - 1.1. The Problem
  - 1.2. Present Work
2. Review of the Previous Work
  - 2.1. Introduction
  - 2.2. Uniform main stream velocity - laminar flow
  - 2.3. Uniform main stream velocity - turbulent flow
  - 2.4. Arbitrary main stream velocity - laminar flow
  - 2.5. Arbitrary main stream velocity - turbulent flow
3. Heat Transfer over a Flat Plate with Arbitrary Heat Flux - Approximate Analysis
  - 3.1. Laminar Flow
  - 3.2. Turbulent Flow
  - 3.3. Approximate Analysis assuming linear temperature profile ( $Pr = 1$ )
4. Numerical Solution for Arbitrary Heat Flux
  - 4.1. Theory
  - 4.2. Numerical Solution
  - 4.3. Form of Presentation in the Results
  - 4.4. Check by heat balance
  - 4.5. Dependence of the Spalding Function and  $\theta$  on the Prandtl Number
  - 4.6. Application of the solutions to the case of arbitrary heat flux at the wall
5. Description of Apparatus
  - 5.1. Introduction
  - 5.2. Air Section
  - 5.3. Diffusing Section
  - 5.4. Test Sections
  - 5.5.  $CO_2$  Section
  - 5.6. Measurements

## **Contents (Continued)**

- 6. Test Procedure - Calculation Procedure**
  - 6.1. Introduction**
  - 6.2. Procedure of Test**
  - 6.3. Preliminary Tests**
  - 6.4. Calculation Procedure (Experimental)**
  - 6.5. Calculation Procedure (Theoretical)**
- 7. Results and Conclusion**
  - 7.1. Results**
  - 7.2. Conclusion**
- 8. References**
- 9. Symbols**
- Figures**

## 1. Introduction

### 1.1. The Problem

The initiation of this investigation was the idea that there might be important advantages in the construction of a solid propellant grain by the assembly of alternate "pineapple rings" of different propellants. This problem was therefore investigated at some length both theoretically and by means of an idealised experiment.

In considering the operation of such a grain, the first problem is that of determining the manner of mixing the gases deriving from the alternate slices.

This problem idealises to the problem of finding mass transfer coefficient and the concentration in the boundary layer for an arbitrary mass diffusing surface. Heat transfer and mass transfer are similar processes with similar differential equations. Therefore, in the case of heat transfer, this is a problem of finding heat transfer and temperature profile in the boundary layer, for non-isothermal surfaces. The present research is a contribution to the solution of this problem.

In the uniform surface temperature case, analytical predictions of the local heat transfer, for laminar flow over a flat plate and wedge, have met with considerable success. When the flow in the boundary layer is turbulent, then the momentum and energy equations for the laminar boundary layer apply with the addition of the eddy transport properties to the viscosity and thermal conductivity. However, these eddy transport properties are not known fundamentally, so that the available solutions are of the analogy type, relating the heat transfer to the friction.

Considerable attention has been directed to the non-uniform wall temperature case, with notable contributions by Lighthill<sup>(5)</sup>, Leveque<sup>(23)</sup>, Rubesin<sup>(15)</sup>, Eckert<sup>(9)</sup>, and Spalding<sup>(8)</sup>, etc. for the laminar case, and by Seban<sup>(12)</sup>, Rubesin<sup>(29)</sup>, etc. for the turbulent case. Reviews of such solutions are given by Tribus and Klein<sup>(6)</sup>, Spalding and Pun<sup>(22)</sup>, and Shah<sup>(37)</sup>.

Although there are numerous methods available for calculating heat transfer over the bodies of arbitrary shape with arbitrary surface temperature, there is no method available for calculating the temperature within the boundary layer.

### 1.2. Present Work

In the present investigation, the theoretical approach to this problem has been made in the field of heat transfer, and the experimental approach is made in the field of mass transfer.

On the theoretical side, the numerical solution of the partial differential equation in the incompressible turbulent boundary layer has been obtained for

step  $\frac{\dot{q}_w''}{\rho u_1 C_p \sqrt{C_f/2}}$  and for Prandtl numbers 0.7, 1 and 7. The Spalding

boundary layer velocity-law was assumed, and the Schmidt method of integration used. Integration was done on a Ferranti Pegasus Digital Computer. A method has been given for applying this solution to the problem of obtaining surface and

fluid temperatures for the case of arbitrary distribution of heat flux at the wall.

Simultaneously, approximate equations for calculating heat transfer over a flat plate with arbitrary heat flux are derived for laminar and turbulent flow. These approximate equations are very simple compared with similar equations of Reynolds et al<sup>(10)</sup>, Rubesin<sup>(15)</sup> etc., and still predict fairly accurate heat transfer coefficients.

To verify the theoretical solution, an experimental rig was designed in which the concentration profiles of the injected gas (carbon dioxide) at different sections were measured when the pipe had another gas (air) flowing turbulently through in the axial direction, and the gas injected was passed through a porous section of the tube wall. The concentration of the carbon dioxide was measured by an Infra-red Gas Analyser.

Designing and manufacturing the experimental rig took a long time. After many modifications, the experimental results obtained were reliable and repeatable.

Experimental results showed higher diffusion when compared with the theoretical solution. In consequence, the experimental concentration of carbon dioxide at the surface was lower by 25% of the theoretical concentration. It seems probable that most of the discrepancy is due to the application of two-dimensional theory to the three-dimensional case of pipe flow.

## 2. Review of the Previous Work

### 2.1. Introduction

In the period of the last ten years, research in the field of heat transfer has increased at a tremendous rate, and numerous investigations are directed to the problem of "heat transfer from non-isothermal surfaces".

The method for determining heat transfer for non-isothermal surfaces is similar to the methods used in determining the deflection of beams subjected to arbitrary load distributions. The energy equation of the boundary layer is linear in the fluid temperature, if the fluid properties are assumed to be constant. This allows the super-position technique to be employed. Rubesin has shown that the heat transfer rate for an arbitrary temperature variation can be determined by superimposing a number of "step temperature distributions", so that the summation of the steps yields the actual variable temperature distribution, and the heat transfer at any point is equal to the sum of the heat transfer rates attributed to all steps upstream of the point in question.

All the approximate methods, instead of satisfying the differential equation for every fluid particle, satisfy boundary conditions near the wall and the region of transition to the external flow, together with certain compatibility conditions. In the remaining region of the fluid in the boundary layer, only an average value over the differential equation is satisfied, the average being taken over the whole thickness of the boundary layer. Such mean values can be obtained from the momentum theory and the law of the conservation of energy. These are, in turn, derived from the equations of motion and energy by integrating over the boundary layer thickness. These integral equations of motion and heat flux, with assumed

velocity and temperature profiles in the boundary layer, form the basis of the approximate methods.

In all cases, if the wall temperature is given, the heat flux is to be calculated from

$$\dot{q}''_{w(x)} = \int_{\xi=0}^{\xi=x} h(\xi, x) dT_w(\xi) \quad (2.1)$$

Here the Kernel function  $h(\xi, x)$  is the heat transfer rate at position  $x$  due to step temperature rise  $\Delta T_w(\xi)$  at the position  $\xi$ . If the heat flux is given, the wall temperature is to be calculated from

$$(T_w - T_i) = \int_{\xi=0}^{\xi=x} g(\xi, x) d\dot{q}''_w(\xi) \quad (2.2)$$

Here the Kernel function  $g(\xi, x)$  is the wall temperature at  $x$  due to unit heat flux at  $\xi$ .

It should be noted that integral of equations 2.1 and 2.2 must be taken in the "Stieltjes" sense rather than in the ordinary "Riemann" or "Area" sense. Various investigators have obtained analytical expressions for the "Kernel" functions, and all these expressions can be divided into four main groups depending on their applicability.

## 2.2. Uniform Main Stream Velocity - Laminar Flow

Leveque<sup>(23)</sup> assumed a linear velocity profile independent of  $x$ , and solved the differential energy equation. He obtained

$$h(\xi, x) = \frac{k(Pr)^{\frac{1}{3}}}{3(\frac{1}{3})!} \left(\frac{\rho}{9\mu}\right)^{\frac{1}{3}} \left[\frac{du}{dy}\right]_{y=0}^{\frac{1}{3}} (x - \xi)^{-\frac{1}{3}} \quad (2.3)$$

Rubesin<sup>(15)</sup> assumed linear velocity and temperature profiles and solved the integral energy equation by further assuming that the thermal boundary layer varies proportionally to the momentum thickness.

He obtained

$$h(\xi, x) = \frac{0.304k}{x} Pr^{\frac{1}{3}} Re_x^{\frac{1}{2}} \left[1 - \left(\frac{\xi}{x}\right)^{\frac{3}{4}}\right]^{-\frac{1}{3}} \quad (2.4)$$

Eckert<sup>(9)</sup> assumed cubic velocity and temperature profiles and solved the integral energy equation. He obtained

$$h(\xi, x) = \frac{0.33k}{x} Pr^{\frac{1}{3}} Re_x^{\frac{1}{2}} \left[1 - \left(\frac{\xi}{x}\right)^{\frac{3}{4}}\right]^{-\frac{1}{3}}$$

Klein and Tribus<sup>(24)</sup> have shown a mathematical manipulation procedure by which the value of  $g(\xi, x)$  can be obtained from the known function  $h(\xi, x)$ . Thus the values of the function  $g(\xi, x)$  obtained from the equations of Leveque<sup>(23)</sup>, Rubesin<sup>(15)</sup> and Eckert<sup>(9)</sup> are

$$g(\xi, x) = \frac{2}{3k} \frac{Pr^{-\frac{1}{3}}}{(\frac{2}{3})!} \left( \frac{\rho}{9\mu} \right)^{-\frac{1}{3}} \left[ \left( \frac{du}{dy} \right)_{y=0} \right]^{-\frac{1}{3}} (x - \xi)^{-\frac{2}{3}} \quad (2.6)$$

$$g(\xi, x) = \frac{1}{6(\frac{1}{3})! (\frac{2}{3})!} \frac{Pr^{-\frac{1}{3}}}{0.304k} Re_x^{-\frac{1}{2}} \left[ 1 - \left( \frac{\xi}{x} \right)^{\frac{3}{4}} \right]^{-\frac{2}{3}} \quad (2.7)$$

and

$$g(\xi, x) = \frac{1}{6(\frac{1}{3})! (\frac{2}{3})!} \frac{Pr^{-\frac{1}{3}}}{0.33k} Re_x^{-\frac{1}{2}} \left[ 1 - \left( \frac{\xi}{x} \right)^{\frac{3}{4}} \right]^{-\frac{2}{3}} \quad (2.8)$$

respectively.

The present authors have assumed cubic velocity and temperature profiles and have obtained a very simple equation for an arbitrary heat flux problem by directly integrating the energy equation for a step heat flux case. Detailed derivation is given in Chapter 3.

### 2.3. Uniform Main Stream Velocity - Turbulent Flow

Rubesin<sup>(11)</sup> assumed velocity and temperature profiles as following a 1/7 power law, and solved the integral energy equation. He obtained

$$h(\xi, x) = \frac{0.0288k}{x} Pr^{\frac{1}{3}} (Re_x)^{0.8} \left[ 1 - \left( \frac{\xi}{x} \right)^{39/40} \right]^{-7/39} \quad (2.9)$$

and

$$g(\xi, x) = \frac{28/195}{(32/39)!(7/39)!} \times \frac{1}{0.0288k} Re_x^{-0.8} x^{0.8} \left[ x^{39/40} - \xi^{39/40} \right]^{-32/39} \dots (2.10)$$

Seban<sup>(12)</sup> followed the same procedure as Rubesin, except that he assumed a linear temperature profile in the laminar sublayer. He obtained

$$h(\xi, x) = \frac{0.0289k}{x} Pr^{1/9} Re_x^{0.8} \left[ 1 - \left( \frac{\xi}{x} \right)^{9/10} \right]^{-1/9} \quad (2.11)$$

and

$$g(\xi, x) = \frac{(8/9)}{(8/9)!(1/9)!} \frac{Pr^{-1/9}}{0.0289k} Re_x^{-0.8} x^{0.8} \left[ x^{9/10} - \xi^{9/10} \right]^{-8/9} \dots (2.12)$$

Maisel and Sherwood<sup>(14)</sup> carried out experimental measurements on a mass transfer apparatus and obtained an empirical equation "best fit" to their data. For air:-

$$h(\xi, x) = \frac{0.035k}{x} Re_x^{0.8} \left[ 1 - \left( \frac{\xi}{x} \right)^{0.8} \right]^{-0.11} \quad (2.13)$$

Reynolds et al<sup>(10)</sup> solved the integral energy equation by assuming velocity and temperature profiles as following 1/7 power law and turbulent Prandtl number equal to unity. They obtained

$$h(\xi, x) = \frac{0.0296k}{x} Pr^{0.6} Re_x^{0.8} \left[ 1 - \left( \frac{\xi}{x} \right)^{9/10} \right]^{-1/9} \quad (2.14)$$

$$\text{and} \quad g(\zeta, x) = \frac{(9/10) \text{Pr}^{-0.4} (\text{Re}_x)^{-0.8}}{\Gamma 1/9 \Gamma 8/9 \cdot 0.0296k} \left[ 1 - \left(\frac{\zeta}{x}\right)^{9/10} \right]^{-8/9} \quad (2.15)$$

For the step heat flux problem, the present authors have derived a simple analytical expression by assuming a seventh power law for velocity and temperature profiles and directly integrating the energy equation. The detailed analysis is given in Section 3.

#### 2.4. Arbitrary Main Stream Velocity - Laminar Flow

Lighthill<sup>(5)</sup> solved the energy equation in Von Mises form, assuming a linear velocity profile in the thermal boundary layer. He obtained

$$h(\zeta, x) = \frac{k}{(\frac{1}{3})!} \text{Pr}^{\frac{1}{3}} \left( \frac{\rho}{9\mu^2} \right)^{\frac{1}{3}} \sqrt{\tau_w(x)} \left[ \int_{\zeta}^x \sqrt{\tau_w(z)} dz \right]^{-\frac{1}{3}} \quad (2.16)$$

and

$$g(\zeta, x) = \frac{2}{9(\frac{1}{3})! k} \cdot \left( \frac{9\mu^2}{\rho \text{Pr}} \right)^{\frac{1}{3}} \frac{1}{\sqrt{\tau_w}} \left[ \int_{\zeta}^x \sqrt{\tau_w(z)} dz \right]^{-\frac{1}{3}} \quad (2.17)$$

Bond<sup>(19)</sup> also assumed a linear velocity profile and solved the differential equation for wedge flow. For the wedge flow ( $u_1 = Ax^m$ ) he obtained

$$h(\zeta, x) = \left[ \frac{1+m}{2} \right]^{\frac{1}{2}} \frac{k}{(\frac{1}{3})! x} b^{\frac{1}{3}} \text{Re}_x^{\frac{1}{3}} \left[ 1 - \left(\frac{\zeta}{x}\right)^c \right]^{-\frac{1}{3}} \quad (2.18)$$

and

$$g(\zeta, x) = \frac{2c}{9(\frac{1}{3})! k} \left( \frac{2}{1+m} \right)^{\frac{1}{2}} b^{-\frac{1}{3}} \text{Re}_x^{-\frac{1}{3}} \left( \frac{x}{\zeta} \right)^{\frac{m+1}{2}} \left[ \frac{x^c - \zeta^c}{\zeta^c} \right]^{-\frac{1}{3}} \quad (2.19)$$

$$\text{where} \quad \left. \begin{aligned} b &= \frac{\text{Pr}}{6} f''_{(0)} \\ c &= 3/4(1+m) \end{aligned} \right\} \quad (2.20)$$

$$f''_{(0)} = \left( \frac{\partial^2 f}{\partial \eta^2} \right)_{\eta=0} \quad \text{is a dimensionless velocity gradient}$$

$$\text{with} \quad \left. \begin{aligned} f &= \sqrt{\frac{m+1}{2}} \frac{y}{\sqrt{u_1 \nu x}} \\ \eta &= \sqrt{\frac{m+1}{2}} \sqrt{\frac{u_1 x}{\nu}} y \end{aligned} \right\} \quad (2.21)$$

Ambrok<sup>(7)</sup> has derived an approximate method for calculating the heat transfer coefficient by assuming that a relation of the type  $\text{Nu} = A \text{Re} (\Delta_s)^n$ , which is valid for a flat plate with a uniform surface temperature, and is also valid for a problem where main stream velocity and surface temperature vary arbitrarily. With this assumption he has solved an integral energy equation. He obtained

$$\frac{\text{Nu}}{\sqrt{\text{Re}}} = \frac{0.332 \text{Pr}^{\frac{1}{3}} (T_w - T_1)}{\left[ \frac{1}{u_1 x} \int_a^x u_1 (T_w - T_1)^2 dx \right]^{\frac{1}{2}}} \quad (2.22)$$

This equation is very simple but it is found to give low values of heat transfer when compared with the exact solution of Eckert for wedge flows.

Spalding<sup>(8)</sup> has improved on Lighthill's method by a correction which accounts for the departure from linearity of the velocity profile within the thermal boundary layer, and which comprehends the influence of Prandtl number, pressure gradient, body forces and non-coincident start of velocity and thermal layers.

In this method, the momentum thickness  $\delta_2$ , of the velocity boundary layer is to be evaluated first by a procedure similar to those of Walz<sup>(26)</sup> and Thwaites<sup>(25)</sup>. With  $\delta_2(x)$  evaluated  $\delta_4(x)$  is to be obtained from a table or graph of  $\delta_4/\delta_2$  vs.  $\frac{\delta_2^2}{\nu} \left( \frac{du_1}{dx} \right)$ . Finally, the heat transfer coefficient is to be obtained from

$$\Delta_4 = \left( \frac{\delta_4}{u_1} \right)^{\frac{1}{2}} \left[ 6.41\alpha \int_a^x \left( \frac{u_1}{\delta_4} \right)^{\frac{1}{2}} dx + \alpha \int_a^x \left( \frac{u_1}{\delta_4} \right)^{\frac{1}{2}} F dx \right] \quad (2.23)$$

where  $F$  is a graphically presented function of the argument  $\frac{\delta_2 \Delta_4}{\nu} \frac{du_1}{dx}$ .

Schuh<sup>(4)</sup> selected a dependent variable, which is a function of the ratio of heat flow across the whole boundary layer to the temperature gradient at the wall in a suitable dimensionless form, and then integrated the momentum and the energy equations.

Schuh's method involves similar steps to those of Spalding's method, namely:-

1. The determination of  $\delta_2$  by the Walz-Thwaites technique.
2.  $\beta$  and  $Z$ , are the functions of  $\frac{\delta_2^2}{\nu} \frac{du_1}{dx}$  and to be read from the graph.
3. Calculation of  $n$  from equation 2.24

$$n = \left( \frac{x}{T_w - T_1} \right) \frac{dT_w}{dx} \quad (2.24)$$

4. Calculation of functions  $G$  and  $P$  from equations 2.25 and 2.27 by an iterative procedure.

$$G = 0.57 (\beta + 0.205)^{0.104} A^{0.37+0.06\beta} (2-\beta)^{\frac{1}{2}} P^{1-3\tau} \quad (2.25)$$

where

$$A = 1 + (2 - \beta) n \quad (2.26)$$

and values of  $\tau$  are to be read from his table.

$$P = \left[ \frac{3}{2Pr} \right]^{\frac{1}{4}} A^{1/6} \frac{1}{\left[ (T_w - T_1) G(2 - \beta) \right]^{\frac{1}{2}} \left[ u_1 x \right]^{\frac{1}{4}}} \times \left[ \int_a^x \left[ \frac{u^\beta}{(2-\beta)x} \right]^{\frac{1}{4}} \frac{G^{3/2} (T_w - T_1)^{3/2}}{A^{\frac{1}{2}}} dx \right]^{\frac{1}{4}} \quad (2.27)$$

5. Heat transfer coefficient then to be calculated from

$$\frac{\Delta_4}{\nu} = \frac{P}{G} \sqrt{\frac{x}{u_1}} \sqrt{2 - \beta} \quad (2.28)$$

Seban<sup>(1)</sup> and Drake<sup>(3)</sup> solved the momentum equation by a procedure similar to that of Eckert, and obtained heat transfer rate by assuming that it is related to the momentum thickness in the same manner as on the wedge.

This method involves similar steps of those of Spalding and Schuh.

1. The determination of  $\delta_2$  and the auxiliary function  $\frac{\delta_2^2}{\nu} \frac{du_1}{dx}$
2. Evaluation of functions  $z_1$  and  $\beta$  from his graph.
3. The rate of heat transfer at the wall for a particular case, when wall temperature is a power function of length, e.g.  $(T_w - T_1) = A x^n$ , is given by

$$\dot{q}_w'' = -k A x^n g'_{(0)} \frac{z_1}{\delta_2} \quad (2.29)$$

or

$$\frac{\Delta_4}{\delta_2} = \frac{1}{g'_{(0)} z_1} \quad (2.30)$$

where  $g'_{(0)}$  is a temperature gradient at the wall.  $g'_{(0)}$  is a function of  $\beta$ ,  $n$  and  $Pr$ . Seban has suggested the exact solutions of Eckert, Levy etc. to be used to obtain the value of  $g'_{(0)}$  for different  $\beta$ ,  $n$  and  $Pr$ .

By superimposing, the heat transfer coefficient can be determined for a variation of the surface temperature of the type

$$(T_w - T_1) = A_1 x^{n_1} + A_2 x^{n_2} + A_3 x^{n_3} + \dots \quad (2.31)$$

2.5. Arbitrary Main Stream Velocity - Turbulent Flow

Very recently Spalding<sup>(16)</sup> has suggested a single analytical formula for velocity distribution throughout the whole of a "Universal" turbulent boundary layer in the form of  $y^+(u^+)$  instead of the usual form  $u^+(y^+)$ . With this form of expression, it is possible to obtain numerical solutions of the partial differential equation for arbitrary surface temperature case and for the arbitrary heat flux case. These solutions cover both the laminar and turbulent flows.

Spalding<sup>(16)</sup> has solved the integral form of the energy equation for step surface temperature and for unity Prandtl number. He assumed a linear temperature profile of the form

$$\left. \begin{array}{ll} u^+ < \delta & ; \quad \theta = 1 - \frac{u^+}{\delta} \\ u^+ > \delta & ; \quad \theta = 0 \end{array} \right\} \quad (2.32)$$

Muralidharan<sup>(17)</sup> has solved the differential equation for step surface temperature and for  $Pr = 0.7, 1$  and  $7$ . He used an analytical formula of Deissler<sup>(32)</sup> for velocity distribution in the boundary layer and obtained the numerical solution on an analogue computer.

Kestin and Persen<sup>(18)</sup> used the digital computer to obtain the numerical solution of the partial differential equation for step surface temperature and for  $Pr = 1$ . They used Spalding's velocity law.

The authors have solved the partial differential equation for arbitrary heat flux problem and for  $Pr = 0.7, 1$  and  $7$ . The detail of the numerical solution is presented in Section 4.

### 3. Heat Transfer over a Flat Plate with Arbitrary Heat Flux. Approximate Analysis

#### 3.1. Laminar Flow

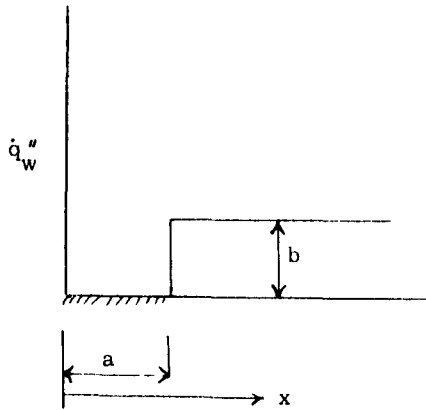


Fig. 3.1

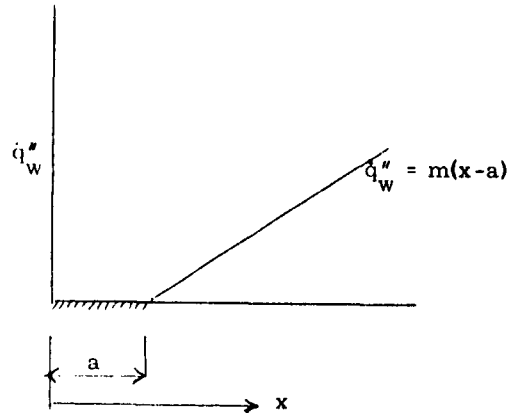


Fig. 3.2

For a step heat flux (Fig. 3.1), total energy at any section  $x$  is:-

$$\dot{q}_w'' (x - a) = \rho u_1 C_p (T_w - T_1) \delta \int_0^{\Delta} \left( \frac{u}{u_1} \right) (1 - \theta) d \left( \frac{y}{\delta} \right) \quad (3.1)$$

For assumed cubic velocity and temperature profiles

$$\left( \frac{u}{u_1} \right) = \frac{3}{2} \left( \frac{y}{\delta} \right) - \frac{1}{2} \left( \frac{y}{\delta} \right)^3 \quad (3.2)$$

$$\theta = \frac{T - T_w}{T_1 - T_w} = \frac{3}{2} \left( \frac{y}{\Delta} \right) - \frac{1}{2} \left( \frac{y}{\Delta} \right)^3 \quad (3.3)$$

Equation 3.1 becomes

$$\dot{q}_w''(x-a) = \rho u_1 C_p (T_w - T_1) \delta \left[ \frac{3}{20} \left( \frac{\Delta}{\delta} \right)^2 - \frac{3}{280} \left( \frac{\Delta}{\delta} \right)^4 \right] \quad (3.4)$$

We are treating the case, that the thermal boundary layer is thinner than the velocity boundary layer, that is  $(\Delta/\delta) < 1$ . The second term in the right-hand expression of equation 3.4 is then small compared with the first, and can be neglected. The heat transfer at the wall is given by

$$\dot{q}_w = h(T_w - T_1) = -k \left[ \frac{\partial T}{\partial y} \right]_{y=0} = \frac{3}{2} \frac{k(T_w - T_1)}{\Delta} \quad (3.5)$$

For a laminar boundary layer, velocity boundary layer thickness is given by:

$$\delta = \frac{4.64 x}{\sqrt{Re}} \quad (3.6)$$

Thus for a step heat flux, from equations 3.4, 3.5 and 3.6 :-

$$(T_w - T_1) = \frac{2.395 b(Re)^{\frac{1}{2}} (Pr)^{\frac{2}{3}}}{\rho u_1 C_p} \left[ 1 - \left( \frac{a}{x} \right) \right]^{\frac{1}{3}} \quad (3.7)$$

and

$$\frac{Nu_x}{\sqrt{Re}} = 0.418 (Pr)^{\frac{1}{3}} \left[ 1 - \left( \frac{a}{x} \right) \right]^{-\frac{1}{3}} \quad (3.8)$$

Where b is the magnitude of the step heat flux.

Similar equations of Eckert<sup>(9)</sup> and Rubesin<sup>(15)</sup> for a step heat flux are

$$(T_w - T_1) = \frac{2.2 b (Re)^{\frac{1}{2}} (Pr)^{\frac{2}{3}}}{\rho u_1 C_p} I_r \left( \frac{1}{3}, 4/3 \right) \quad (3.9)$$

and

$$(T_w - T_1) = \frac{2.405 b (Re)^{\frac{1}{2}} (Pr)^{\frac{2}{3}}}{\rho u_1 C_p} I_r \left( \frac{1}{3}, 4/3 \right) \quad (3.10)$$

respectively. It can be seen that equation 3.7 is relatively simple, for it does not contain the incomplete beta function. For any arbitrary heat flux, the wall temperature and the heat transfer coefficient can be calculated by superimposing small steps. Thus for any arbitrary heat flux

$$(T_w - T_1) = \frac{2.395 Re^{\frac{1}{2}} Pr^{\frac{2}{3}}}{\rho u_1 C_p} \int_{\xi=0}^{\xi=x} (1 - \xi/x)^{\frac{1}{3}} \frac{d \dot{q}_w''(\xi)}{d\xi} d\xi \quad (3.11)$$

and

$$\frac{Nu_x}{\sqrt{Re}} = \frac{0.418 (Pr)^{\frac{1}{3}} \dot{q}_w''(x)}{\int_{\xi=0}^{\xi=x} (1 - \xi/x)^{\frac{1}{3}} \frac{d \dot{q}_w''(\xi)}{d\xi} d\xi} \quad (3.12)$$

It should be noted that the integral of 3.11 and 3.12 must be taken in the "Stieltjes" sense. For instance, for a delayed ramp heat flux (Fig. 3.2):

$$(T_w - T_1) = \frac{1.797 (Re)^{\frac{1}{2}} (Pr)^{\frac{2}{3}} mx}{\rho u_1 C_p} \left[ 1 - (a/x) \right]^{4/3} \quad (3.13)$$

and

$$\frac{Nu_x}{\sqrt{Re}} = 0.557 (Pr)^{\frac{1}{3}} \left[ 1 - (a/x) \right]^{-\frac{1}{3}} \quad (3.14)$$

### 3.2. Turbulent Boundary Layer

For a step heat flux, in the turbulent boundary layer, we assume velocity and temperature profiles :-

$$\left( \frac{u}{u_1} \right) = (y/\delta)^{1/7} \quad (3.15)$$

and

$$\theta = \frac{T - T_w}{T_1 - T_w} = (y/\Delta)^{1/7} \quad (3.16)$$

Then equation 3.1 becomes

$$\dot{q}_w'' (x - a) = \rho u_1 C_p (T_w - T_1) \delta \left[ \frac{7}{72} \left( \frac{\Delta}{\delta} \right)^{8/7} \right] \quad (3.17)$$

The heat transfer momentum analogy derived by Reynolds et al<sup>(10)</sup>, for step heat flux is:-

$$St_x = \frac{\dot{q}_w''}{(T_w - T_1) \rho u_1 C_p} = \frac{C_f}{2} \left( \frac{\Delta}{\delta} \right)^{-1/7} \quad (3.18)$$

where the Prandtl number dependence factor is applied afterwards.

For a turbulent boundary layer

$$\frac{C_f}{2} = 0.0296 (Re)^{-0.2} \quad (3.19)$$

$$\frac{\delta}{x} = 0.37 (Re)^{-0.2} \quad (3.20)$$

Thus for a step heat flux, from equations 3.17, 3.18, 3.19 and 3.20 :-

$$(T_w - T_1) = \frac{32.95 b}{\rho C_p u_1} (Re)^{0.2} (Pr)^{0.4} (1 - a/x)^{1/9} \quad (3.21)$$

and

$$\frac{Nu_x}{(Re)^{0.8}} = 0.03035 (Pr)^{0.6} (1 - a/x)^{-1/9} \quad (3.22)$$

where b is the magnitude of the step heat flux. The similar equation of Reynolds et al<sup>(10)</sup>

for a step heat flux is:-

$$(T_w - T_f) = 32.42 \frac{b}{\rho C_p u_f} (Re)^{0.2} (Pr)^{0.4} I_B(1/9, 10/9) \quad (3.23)$$

Equation 3.21 is relatively simple, for it does not contain the incomplete beta function. For any arbitrary heat flux, the wall temperature and the heat transfer coefficient can be calculated by superimposing small steps. Thus for any arbitrary heat flux:-

$$(T_w - T_f) = \frac{32.95 (Re)^{0.2} (Pr)^{0.4}}{\rho C_p u_f} \int_{\xi=0}^{\xi=x} (1 - \xi/x)^{1/9} \frac{d\dot{q}_w''(\xi)}{d\xi} d\xi \quad (3.24)$$

and

$$\frac{Nu_x}{(Re)^{0.8}} = \frac{0.03035 (Pr)^{0.6} \dot{q}_w''(x)}{\int_{\xi=0}^{\xi=x} (1 - \xi/x)^{1/9} \frac{d\dot{q}_w''(\xi)}{d\xi} d\xi} \quad (3.25)$$

In equations 3.24 and 3.25 the integral must be taken in the "Stieltjes" sense. Taking a delayed ramp heat input (Fig. 3.2) as an example:-

$$(T_w - T_f) = \frac{29.65 m x (Pr)^{0.4} (Re)^{0.2}}{\rho C_p u_f} (1 - a/x)^{10/9} \quad (3.26)$$

and

$$\frac{Nu_x}{(Re)^{0.8}} = 0.03373 (Pr)^{0.6} (1 - a/x)^{-1/9} \quad (3.27)$$

Results of the above equations are compared with Reynolds et al<sup>(10)</sup> Eckert<sup>(9)</sup>, and Rubesin<sup>(15)</sup>, for both laminar and turbulent boundary layers, and are plotted in Figs. 3.3 and 3.4.

For the laminar case, the results of the above equations agree very well with that of Rubesin<sup>(15)</sup>, and not with Eckert<sup>(9)</sup>. The disagreement with Eckert is merely in a numerical factor. Eckert's  $(T_w - T_f)$  values are 8% lower than those of equation 3.7.

For the turbulent case, the results agree within 1.5% to that of Reynolds et al<sup>(10)</sup>.

### 3.3. Approximate Analysis assuming Linear Temperature Profile (Pr = 1)

For a step heat flux, total energy at any section  $x$  is:

$$\dot{q}_w''(x-a) = \int_0^{\infty} \rho C_p u (T - T_1) dy \quad (3.28)$$

or

$$St(x-a)u_1 = \int_0^{\infty} u \theta dy \quad (3.29)$$

With

$$x^{+'} = \left( \frac{x-a}{\nu} \right) \sqrt{\frac{r_w}{\rho}} = \frac{(x-a)}{\nu} u_1 \sqrt{\frac{C_f}{2}} \quad (3.30)$$

$$y^{+} = \frac{y}{\nu} \sqrt{\frac{r_w}{\rho}} = \frac{u_1 y}{\nu} \sqrt{\frac{C_f}{2}} \quad (3.31)$$

$$u^{+} = \frac{u}{\sqrt{\frac{r_w}{\rho}}} = \frac{u}{u_1} \times \frac{1}{\sqrt{\frac{C_f}{2}}} \quad (3.32)$$

and

$$\frac{dy^{+}}{du^{+}} = \epsilon^{+} \quad (3.33)$$

equation 3.29 simplifies to:

$$\frac{St}{\sqrt{\frac{C_f}{2}}} x^{+'} = \int_0^{\delta} u^{+} \theta \epsilon^{+} du^{+} \quad (3.34)$$

Assuming a linear temperature profile

$$\theta = 1 - \frac{u^{+}}{\delta} \quad (3.35)$$

and knowing that

$$\frac{St}{\sqrt{\frac{C_f}{2}}} = - \left( \frac{\partial \theta}{\partial u^{+}} \right)_{u^{+}=0} \quad (3.36)$$

Equation 3.34 simplifies to:

$$\frac{x^{+}}{\delta} = \int_0^{\delta} u^{+} \left( 1 - \frac{u^{+}}{\delta} \right) \epsilon^{+} du^{+} \quad (3.37)$$

From Spalding's<sup>(16)</sup> velocity profile:-

$$\epsilon^{+} = 1 + \frac{k'}{E} \left[ e^{k'u^{+}} - 1 - k'u^{+} - \frac{(k'u^{+})^2}{2!} - \frac{(k'u^{+})^3}{3!} \right] \quad (3.38)$$

with  $k' = 0.407$   
and  $\frac{1}{E} = 0.0991$

From equations 3.37 and 3.38

$$\begin{aligned} \frac{x^{+'}}{\delta} = & \frac{\delta^2}{6} \left(1 - \frac{k'}{E}\right) + \frac{k'}{E} \left[ \frac{e^{k'\delta}}{k'^2} \left(1 - \frac{2}{k'\delta}\right) + \frac{1}{k'^2} \left(1 + \frac{2}{k'\delta}\right) \right. \\ & \left. - \frac{k'\delta^3}{6} \left[ \frac{1}{2} + \frac{3}{20} k'\delta + \frac{k'\delta^2}{30} \right] \right] \end{aligned} \quad (3.39)$$

Equation 3.39 is compared with previous approximate analyses for laminar and turbulent flows obtained by assuming cubic and seventh power profiles respectively. (Eqs. 3.42 and 3.45). Comparison is shown in Fig. 3.5 and agreement is found to be very satisfactory.

For  $Pr = 1$ , equation 3.8 of laminar flow is:

$$\frac{Nu}{\sqrt{Re}} = 0.418 (1 - 9/x)^{-\frac{1}{3}} \quad (3.40)$$

Knowing  $\frac{C_f}{2} = \frac{0.332}{\sqrt{Re}} \quad (3.41)$

for laminar flow, equation 3.40 simplifies to:

$$\frac{St}{\sqrt{\frac{C_f}{2}}} = 0.603 x^{+'}^{-\frac{1}{3}} \quad (3.42)$$

For  $Pr = 1$ , equation 3.22 of turbulent flow is:

$$\frac{Nu}{Re^{0.8}} = 0.03035 (1 - 9/x)^{-1/9} \quad (3.43)$$

with

$$\frac{C_f}{2} = 0.0296 Re^{-0.2} \quad (3.44)$$

equation 3.43 simplifies to:

$$\frac{St}{\sqrt{\frac{C_f}{2}}} = 0.1452 x^{+'}^{-1/9} \quad (3.45)$$

#### 4. Numerical Solution for Arbitrary Heat Flux

##### 4.1. Theory

By use of the Von Mises transformation, Spalding<sup>(16)</sup> has reduced the energy equation for a turbulent incompressible boundary layer

$$u \frac{\partial T}{\partial x} + v \frac{\partial T}{\partial y} = \frac{\partial}{\partial y} \left[ \alpha \frac{\partial T}{\partial y} + \epsilon_h \frac{\partial T}{\partial y} \right] \quad (4.1)$$

to

$$\frac{\partial T}{\partial x^+} = \frac{1}{\epsilon^+ u^+} \frac{\partial}{\partial u^+} \left[ \frac{\alpha^+}{\epsilon^+} \frac{\partial T}{\partial u^+} \right] \quad (4.2)$$

where

$$x^+ = \int_a^x \sqrt{\frac{r_w}{\rho}} \frac{u_r}{\nu} dx = \int_a^x \frac{u_r}{\nu} dx \quad (4.3)$$

$$y^+ = \sqrt{\frac{r_w}{\rho}} y = \frac{u_r y}{\nu} \quad (4.4)$$

$$u^+ = \frac{u}{\sqrt{\frac{r_w}{\rho}}} = \frac{u}{u_r} \quad \text{and} \quad u^+ = u^+(y^+) \quad (4.5)$$

$$\epsilon^+ = 1 + \frac{\epsilon}{\nu} = \frac{dy^+}{du^+} \quad (4.6)$$

(this implies that shear stress is independent of  $y$ )

$$\alpha^+ = \frac{1}{Pr} + \frac{\epsilon_h}{\nu} \quad (4.7)$$

Further, using a new variable  $\xi$  defined by  $d\xi = \frac{\epsilon^+}{\alpha^+} du^+$  equation 4.2 can be reduced to

$$\frac{\partial T}{\partial x^+} = \frac{1}{u^+ \alpha^+} \frac{\partial^2 T}{\partial \xi^2} \quad (4.8)$$

with boundary conditions

$$\begin{aligned} T &= 0 \quad \text{at} \quad \xi = \infty \\ \text{and} \quad T &= 0 \quad \text{at} \quad x^+ \leq 0 \end{aligned} \quad (4.10)$$

In this section the temperatures  $T$  and  $T_w$  are relative to the fluid temperature  $T_1$ .

An additional boundary condition in the present solution is

$$\left( \frac{\partial T}{\partial \xi} \right)_{\xi=0} = \text{Constant} \quad (4.11)$$

Spalding<sup>(16)</sup> has derived a single expression for the distribution of the velocity in the universal turbulent boundary layer in the form of  $y^+$  ( $u^+$ ) instead of the usual form  $u^+(y^+)$ . It is: -

$$y^+ = u^+ + \frac{1}{E} \left\{ e^{k'u^+} - 1 - k'u^+ - \frac{(k'u^+)^2}{2!} - \frac{(k'u^+)^3}{3!} - \frac{(k'u^+)^4}{4!} \right\} \quad (4.12)$$

where  $k' = 0.407$

and  $1/E = 0.0991$

From equation 4.12 an expression for  $\epsilon^+$  can be obtained, using equation 4.6. This gives

$$\epsilon^+ = 1 + \frac{k'}{E} \left\{ e^{k'u^+} - 1 - k'u^+ - \frac{(k'u^+)^2}{2!} - \frac{(k'u^+)^3}{3!} \right\} \quad (4.13)$$

A further assumption that the turbulent Prandtl number is unity ( $\epsilon_h = \epsilon$ ) leads to an expression for  $\alpha^+$

$$\alpha^+ = \frac{1}{Pr} + \frac{k'}{E} \left\{ e^{k'u^+} - 1 - k'u^+ - \frac{(k'u^+)^2}{2!} - \frac{(k'u^+)^3}{3!} \right\} \quad (4.14)$$

Therefore the quantity  $(u^+ \alpha^+)$ , for various Prandtl numbers, can be obtained as a function of  $\xi$ . This reduces equation 4.9 to

$$\frac{\partial T}{\partial x^+} = \frac{1}{f(\xi)} \frac{\partial^2 T}{\partial \xi^2} \quad (4.15)$$

The values of  $f(\xi)$  for  $Pr = 0.7, 1$  and  $7$  are shown in Fig. 4.6.

For the uniform surface temperature case, various investigators have solved equation 4.15. Spalding<sup>(16)</sup> has solved it approximately for  $Pr = 1$ , by use of the energy integral equation and assuming a temperature profile in the boundary layer. Muralidharan<sup>(17)</sup> has solved it on an analogue computer for  $Pr = 0.7, 1$  and  $7$ . Kestin and Persen<sup>(18)</sup> have solved it on a digital computer for  $Pr = 1$ .

In the present paper, a solution of equation 4.15 has been made for uniform  $\left(\frac{\partial T}{\partial \xi}\right)$  at the wall and for  $Pr = 0.7, 1$  and  $7$ .

#### 4.2. Numerical Solution

It will be seen that equation 4.15 is very similar to the heat conduction equation, and may be solved by the finite difference method of E. Schmidt.

The equation 4.15 can be written in finite-difference form as

$$T_{(x^+ + \Delta x^+, \xi)} - T_{(x^+, \xi)} = \frac{\Delta x^+}{f(\xi) (\Delta \xi)^2} \left[ T_{(x^+, \xi + \Delta \xi)} + T_{(x^+, \xi - \Delta \xi)} - 2T_{(x^+, \xi)} \right] \quad (4.16)$$

From equation 4.16,  $T_{(x^+ + \Delta x^+)}$  can be calculated from  $T_{(x^+)}$  which in turn can be calculated from  $T_{(x^+ - \Delta x^+)}$  and so on. The grid for the finite difference scheme is shown in Fig. 4.7.

From Fig. 4.7 it can be seen that all the values of temperature can be calculated for  $T_{(x^+ + \Delta x^+)}$  from  $T_{(x^+)}$  except two end values, one at the wall and the second at  $\xi = \xi_{\max}$ . The latter difficulty was met by selecting  $\xi_{\max}$  so high that  $T$  there was zero. The value of  $T$  at the wall was obtained by adding the wall temperature gradient  $\times \Delta \xi$  to the value of the temperature at  $(x^+ + \Delta x^+, \Delta \xi)$ .

To obtain the numerical results in solving equation 4.15, the complete calculations were made for an arbitrary value  $\left(\frac{\partial T}{\partial \xi}\right)_{\xi=0} = -40$ , and later the results were made dimensionless. The number -40 has no particular significance.

It was not possible to start the solution at  $x^+ = 0$  because temperature at all values of  $\xi$  at  $x^+ = 0$  were zero. This difficulty was overcome by starting the solution at a very low value of  $x^+$  called  $x_1^+$ .

The starting value of  $x_1^+$  for  $\left(\frac{\partial T}{\partial \xi}\right)_{\xi=0} = -40$  was selected such that the temperature at all values of  $\xi$  was zero except at the surface. This first-assumed value of the surface temperature  $T_{w_1}$  was obtained from the approximate analysis of Smith and Shah<sup>(35)</sup>. The final results when checked by integrating the heat flux showed that they were not affected by any error in this assumption. The starting values for various Prandtl numbers are tabulated in Table 4.1.

Pr	$T_{w_1}$	$x_1^+$	$\Delta \xi$
0.7	19.30	0.050	0.5
1.0	19.41	0.025	0.5
7.0	38.50	0.004	1.0

Table 4.1

The solution by the method of E. Schmidt is stable only if the condition

$$\frac{\Delta x^+}{f(\xi) (\Delta \xi)^2} < \frac{1}{2} \quad (4.17)$$

is fulfilled throughout. Since it was decided to solve the equation up to  $x^+ = 10^6$ , the interval  $\Delta x^+$  was increased gradually as shown in Tables 4.2, 4.3 and 4.4. With the increase in the interval  $\Delta x^+$ , it became necessary to increase  $\Delta \xi$  near the surface (low values of  $\xi$ ) to fulfil the above condition.

As the values of  $f(\xi)$  increase with  $\xi$  the interval  $\Delta\xi$  was gradually reduced for the calculations away from the surface. Near the surface, the temperature profile gradually became linear and therefore this increase in  $\Delta\xi$  near the wall, with the increase in the interval  $\Delta x^+$  did not impair the accuracy of the final results.

Interval $x^+$	$\Delta x^+$	Min. $\Delta\xi$	Max. $\Delta\xi$
0 to 1	0.05	0.5	0.5
1 to 10	0.1	0.5	0.5
10 to $10^2$	1	0.5	1
$10^2$ to $10^3$	1	0.5	1
$10^4$ to $10^5$	50	0.5	4
$10^5$ to $10^6$	500	0.5	8

Table 4.2. Steps chosen for  $Pr = 0.7$

Interval $x^+$	$\Delta x^+$	Min. $\Delta\xi$	Max. $\Delta\xi$
0 to 1	0.025	0.5	0.5
1 to 10	0.5	1	1
10 to $10^2$	1	1	1
$10^2$ to $10^3$	4	1	2
$10^3$ to $10^4$	20	1	4
$10^4$ to $10^5$	25	1	4
$10^5$ to $10^6$	250	1	8

Table 4.3. Steps chosen for  $Pr = 1$

Interval $x^+$	$\Delta x^+$	Min. $\Delta\xi$	Max. $\Delta\xi$
0 to 1	0.005	1	1
1 to 10	0.05	1	2
10 to $10^2$	0.5	1	4
$10^2$ to $10^3$	1	2	6
$10^3$ to $10^4$	5	2	8
$10^4$ to $10^5$	25	2	14

Table 4.4. Steps chosen for  $Pr = 7$

#### 4.3. Form of Presentation in the Results

The numbers resulting from the computations are temperature differences  $T$  in  $\xi$ ,  $x^+$  co-ordinates, with  $\left(\frac{\partial T}{\partial \xi}\right)_{\xi=0} = -40$ . Heat transfer coefficients may be computed conveniently from such results in terms of the "Spalding function"  $St/\sqrt{C_f/2}$ , by the relation, deduced from equations 4.4, 4.8 and 4.12.

$$\frac{St}{\sqrt{\frac{C_f}{2}}} = - \left( \frac{\partial T}{\partial \xi} \right)_{\xi=0} / T_w \quad (4.18)$$

Thus  $St/\sqrt{C_f/2} (x^+)$  can be presented.

Note, further, that

$$\frac{St}{\sqrt{\frac{C_f}{2}}} = \frac{\dot{q}_w''}{\rho C_p u_i \sqrt{C_f/2}} \times \frac{1}{T_w} \quad (4.19)$$

Assuming that  $C_f/2 (x)$  and  $u_i(x)$  are known for a specific example,  $x^+(x)$  may be computed from equation 4.3. Hence from  $St/\sqrt{C_f/2} (x^+)$ ,  $St(x)$  may be computed. Then knowing the constant value of  $\dot{q}_w'' / \rho u_i C_p \sqrt{C_f/2}$ ,  $T_w$  may be found. Treatment for arbitrary  $\dot{q}_w''$  is given in a later section.

For the temperature within the boundary layer, it will then suffice if  $\theta(\xi, x^+)$  be presented.

A practicable presentation is thus of  $St/\sqrt{C_f/2} (x^+)$  and  $\theta(\xi, x^+)$ .

#### 4.4. Check by Heat Balance

An integral form of the equation 4.15 may be derived by integrating it along the  $\xi$  co-ordinate. Thus

$$\frac{d}{dx^+} \int_0^\infty T u^+ \alpha^+ d\xi = - \left( \frac{\partial T}{\partial \xi} \right)_{\xi=0} \quad (4.20)$$

In our solution  $\left( \frac{\partial T}{\partial \xi} \right)_{\xi=0} = \text{Constant}$  and therefore

$$\int_0^\infty T u^+ \alpha^+ d\xi = - \left( \frac{\partial T}{\partial \xi} \right)_{\xi=0} x^+ \quad (4.21)$$

Therefore from equations 4.18 and 4.21 we have

$$\int_0^\infty \theta u^+ \alpha^+ d\xi = \frac{St}{\sqrt{\frac{C_f}{2}}} x^+ \quad (4.22)$$

The temperature profiles obtained in the numerical solution were integrated at various sections and the integrated heat fluxes were compared with the Spalding function and  $x^+$  as shown in equation 4.22. Comparisons for various Prandtl numbers are tabulated in tables 4.5, 4.6 and 4.7. The results were found reasonably satisfactory.

#### 4.5. Dependence of the Spalding function and $\theta$ on the Prandtl number

The results of the calculations in terms of the temperature profiles are shown in Figs. 4.1, 4.2, and 4.3. The values of the Spalding function for various values of  $x^+$  and for Prandtl number 0.7, 1 and 7, are tabulated in Tables 4.8, 4.9 and 4.10 and plotted in Fig. 4.4.

Having performed these calculations and checks, an effort was made to find the dependence on Prandtl number of the Spalding function and the temperature profile in the form

$$\frac{St}{\sqrt{\frac{C_f}{2}}} = \left( \frac{St}{\sqrt{\frac{C_f}{2}}} \right)_{Pr=1} \times Pr^n \quad (4.23)$$

Results for  $Pr = 0.7, 1$  and  $7$  showed that in the laminar region (up to  $x^+ = 1000$ ) the value of  $n$  remains constant and is equal to  $-2/3$ , but for higher  $x^+$ , the value of  $n$  when obtained from the results for  $Pr = 0.7$  and  $1$ , changes from  $-2/3$  at  $x^+ = 1000$  to  $-0.4$  at  $x^+ = 10^5$  and  $-0.325$  at  $x^+ = 10^6$ , whereas from the results for  $Pr = 7$ , the value of  $n$  decreases from  $-2/3$  at  $x^+ = 1000$  to  $-0.516$  at  $x^+ = 10^5$ .

In the laminar region ( $x^+ < 1000$ ) the temperature profile for any Prandtl number can be obtained from

$$\theta(\xi) = \theta(\xi') (Pr=1) \quad (4.24)$$

where

$$\xi = \xi' \times Pr^{2/3} \quad (4.25)$$

Temperature profiles for various Prandtl numbers and for  $x^+ = 100$  are shown in Fig. 4.5.

#### 4.6. Application of the Solutions to the Case of Arbitrary Heat Flux at the Wall

The working equation by which the numerical solutions given in this paper may be applied is equation 4.33 below. A full statement of its development is given in Sections (a) and (b) following.

##### (a) Determination of temperature at the wall.

The numerical solutions given in the previous sections have the boundary condition  $\left( \frac{\partial T}{\partial \xi} \right)_{\xi=0} = \text{constant}$ ,  $x^+ > 0$ . From the definitions of the variables

in equations 4.8, 4.7, 4.6 and earlier, together with the velocity-law equation 4.12, this boundary condition is the same as  $\dot{q}_w'' / \rho u, C_p \sqrt{C_f/2} = \text{constant}$ .

That is, the heat flux parameter is constant.

This boundary condition is highly particular: usually problems will be met in the form of a specified distribution of  $\dot{q}_w''$ , with  $T_w(x)$  the quantity desired to be known.

However, the treatment of the problem of arbitrary  $\dot{q}_w''$  will be most easily perceived after a recapitulation of the method of determination of  $T_w(x)$  for constant  $\dot{q}_w'' / \rho u_1 C_p \sqrt{C_f/2}$ .

Fig. 4.4 gives values of the Spalding function  $St/\sqrt{C_f/2}$  ( $Pr, x^+$ ). If  $St/\sqrt{C_f/2}$  be known at a given  $x$ , then  $T_w$  is given by

$$T_w = \frac{1}{St/\sqrt{C_f/2}} \times \left( \frac{\dot{q}_w''}{\rho u_1 C_p \sqrt{C_f/2}} \right) \quad (4.26)$$

In Fig. 4.4, heat injection starts at  $x = a$ . We set the problem, then, of calculation of the temperature  $T_{w(b)}$  at  $x = b$ , consequent on constant  $\dot{q}_w'' / \rho u_1 C_p \sqrt{C_f/2}$  between  $x = a$  and  $x = b$ .

Define a new variable  $x_{a,b}^+$  by the equation

$$x_{a,b}^+ = \int_a^b \frac{\sqrt{\tau_w/\rho}}{\nu} dx \quad (4.27)$$

Then  $x_{a,b}^+$  is easily calculable, knowing  $\tau_w, \rho$  and  $\nu$ . From Fig. 4.4 ( $St/\sqrt{C_f/2}$ ) $_{a,b}$  may be read off, for  $x^+ = x_{a,b}^+$ . This quantity is the value of  $St/\sqrt{C_f/2}$  at  $x = b$  consequent on constant  $\dot{q}_w'' / \rho u_1 C_p \sqrt{C_f/2}$  from  $x = a$  to  $x = b$ . Then at  $x = b$ , the difference  $T_{w(b)}$  between wall temperature and mainstream is given by

$$T_{w(b)} = \frac{1}{\left( St/\sqrt{C_f/2} \right)_{a,b}} d \left( \frac{\dot{q}_w''}{\rho u_1 C_p \sqrt{C_f/2}} \right) \quad (4.28)$$

It must be particularly noted that equation 4.28 holds for constant

$\dot{q}_w'' / \rho u_1 C_p \sqrt{C_f/2}$  between  $x = a$  and  $x = b$ . However, in the general problem,  $\dot{q}_w'' / \rho u_1 C_p \sqrt{C_f/2}$  will be a function of  $x$ . Knowing  $\dot{q}_w''(x)$ ,  $u_1(x)$  and  $C_f(x)$  the dependence of  $\dot{q}_w'' / \rho u_1 C_p \sqrt{C_f/2}$  on  $x$  may be computed. The temperature at the wall at  $x = b$  is then given by the Stieltjes integral.

$$T_{w(b)} = \int_0^b \frac{1}{\left( St/\sqrt{C_f/2} \right)_{a,b}} d \left( \frac{\dot{q}_w''}{\rho u_1 C_p \sqrt{C_f/2}} \right)_a \quad (4.29)$$

Equation 4.29 is the working equation for the determination of wall temperature. In equation 4.29,  $(St/\sqrt{C_f/2})_{a,b}$  is the value of  $St/\sqrt{C_f/2}$  at  $b_w$  consequent on constant  $\dot{q}_w''/\rho u_i C_p \sqrt{C_f/2}$  between  $x = a$  and  $x = b$ .  $d \left( \frac{\dot{q}_w''}{\rho u_i C_p \sqrt{C_f/2}} \right)$  is the increment of heat flux parameter for the increment  $dx$  containing  $x = a$ . It may be more convenient for computation if equation 4.29 is re-written.

$$T_{w(b)} = \int_0^b \frac{1}{\left( \frac{St}{\sqrt{C_f/2}} \right)_{a,b}} \frac{d}{dx} \left( \frac{\dot{q}_w''}{\rho u_i C_p \sqrt{C_f/2}} \right)_a dx \quad (4.30)$$

In evaluating equation 4.30, however, it must be noted that if there is a step in  $\dot{q}_w''/\rho u_i C_p \sqrt{C_f/2}$ , this step contributes an increment of  $T_{w(b)}$  given by

$$\Delta T_{w(b)} = \left( \frac{1}{\left( \frac{St}{\sqrt{C_f/2}} \right)_{a,b}} \right) \Delta \left( \frac{\dot{q}_w''}{\rho u_i C_p \sqrt{C_f/2}} \right)_a \quad (4.31)$$

In equation 4.31 the symbol  $\Delta$  signifies a finite increment.

(b) Determination of temperature within the boundary layer.

The previous section showed the method of computing wall temperature consequent on an arbitrary distribution of wall heat flux. A further problem is, however, the determination of temperature within the boundary layer. Again the method will be seen more easily if the computation for step  $\dot{q}_w''/\rho u_i C_p \sqrt{C_f/2}$  is first considered.

Temperatures within the boundary layer have been presented in Figs. 4.1, 4.2, and 4.3 as  $\theta(x^+, \xi, Pr)$ .  $\theta$ , defined as in the list of notation, is in fact temperature on a scale such that mainstream temperature is zero and wall temperature is unity. The temperature at a point in the boundary layer is defined if  $T_w$  and  $\theta$  be known. The relation is  $T = \theta T_w$ .

Concentrating our attention on the case of constant  $\dot{q}_w''/\rho u_i C_p \sqrt{C_f/2}$ , the temperature difference between wall and mainstream at  $x = b$ , called  $T_{w(b)}$ , may be found by the method of the previous section. The problem now is to find the fluid temperature at point  $c$  with co-ordinates  $x, y$ . Of the parameters in Figs. 4.1, 4.2 and 4.3,  $x^+$  and  $Pr$  are already known. To determine  $\theta$  and thus permit the determination of temperature at  $y$ , the dimensionless co-ordinate  $\xi$  must be determined for the point  $c$ .  $\xi$  is defined by equation 4.8 and equations 4.8, 4.7, 4.6, 4.5, 4.12, 4.13 and 4.14 permit the function  $\xi(y^+, Pr)$  to be computed. Results of this computation are shown in Fig. 4.8 and Table 4.11. Using Fig. 4.8,  $\xi$  may therefore be found, after  $y^+$  has been determined from equation 4.4. Thence  $\theta$  may be read off Figs. 4.1, 4.2 or 4.3. The difference of temperature between point  $c$  and the mainstream is then

$$T_{c(b)} = \frac{\theta(a, b, c)}{\left( \frac{St}{\sqrt{C_f/2}} \right)_{a,b}} \left( \frac{\dot{q}_w''}{\rho u_i C_p \sqrt{C_f/2}} \right) \quad (4.32)$$

In equation 4.32,  $\theta_{(a,b,c)}$  is the value of  $\theta$  at  $x^+ = x_{a,b}^+$  and the appropriate  $\xi$ .  $(St/\sqrt{C_f/2})_{a,b}$  is the value read off Fig. 4.4 at  $x^+ = x_{a,b}^+$  and  $\dot{q}_w''/\rho u_p C_p \sqrt{C_f/2}$  is the constant value of the heat flux parameter between  $x = a$  and  $x = b$ .

When there is an arbitrary distribution  $\dot{q}_w''(x)$  the distribution of the heat flux parameter may be computed as described in the previous section of the paper, and the value of the difference in temperature between point  $c$  and the mainstream computed by the Stieltjes integral:

$$T_{c(b)} = \int_0^b \frac{\theta_{(a,b,c)}}{\left(\frac{St}{\sqrt{C_f/2}}\right)_{a,b}} d \left( \frac{\dot{q}_w''}{\rho u_p C_p \sqrt{C_f/2}} \right)_a \quad (4.33)$$

Equation 4.33 is the general equation by which the results of this paper may be applied, since it comprehends equation 4.29 in that at the wall,  $\theta$  is unity. Again it may be more convenient for computation if the equation is rewritten

$$T_{c(b)} = \int_0^b \frac{\theta_{(a,b,c)}}{\left(\frac{St}{\sqrt{C_f/2}}\right)_{a,b}} \frac{d}{dx} \left[ \frac{\dot{q}_w''}{\rho u_p C_p \sqrt{C_f/2}} \right]_a dx \quad (4.34)$$

In the evaluation of equation 4.34 care must be taken in allowing for steps in  $\dot{q}_w''/\rho u_p C_p \sqrt{C_f/2}$  as was pointed out after equation 4.30.

$x^+$	$\frac{St}{\sqrt{C_f/2}} \quad x^+$	$\int_0^\infty \theta u^+ \alpha^+ d\xi$	% diff.
10	3.810	3.838	+ 0.72
$10^2$	17.97	18.07	+ 0.54
$10^3$	97.15	97.21	+ 0.05
$10^4$	653.6	652.4	- 0.18
$10^5$	4952	4876	- 1.54
$10^6$	39660	39780	+ 0.30

Table 4.5 Integrated Check of the Results for  $Pr = 0.7$

$x^+$	$\frac{St}{\sqrt{C_f/2}} x^+$	$\int_0^\infty \theta u^+ \alpha^+ d\xi$	% diff.
10	2.965	3.010	+ 1.51
$10^2$	14.18	14.22	+ 0.30
$10^3$	77.28	77.48	+ 0.27
$10^4$	544.1	546.6	+ 0.44
$10^5$	4293	4298	+ 0.11
$10^6$	35320	35190	- 0.37

Table 4.6 Integrated Check of the Results for Pr = 1

$x^+$	$\frac{St}{\sqrt{C_f/2}} x^+$	$\int_0^\infty \theta u^+ \alpha^+ d\xi$	% diff.
10	0.8185	0.7994	- 2.33
$10^2$	3.844	3.856	+ 0.31
$10^3$	20.75	20.57	- 0.87
$10^4$	171.3	171.2	- 0.06
$10^5$	1571	1579	+ 0.52

Table 4.7 Integrated Check of the Results for Pr = 7

$x^+$	$\frac{St}{\sqrt{C_f/2}}$		$x^+$	$\frac{St}{\sqrt{C_f/2}}$
0				
1	0.801678		$1.10^3$	0.097158
2	0.642647		2	0.084421
3	0.563886		3	0.078568
4	0.513691		4	0.074916
5	0.477754		5	0.072325
6	0.450215		6	0.070346
7	0.428144		7	0.068760
8	0.409884		8	0.067446
9	0.394414		9	0.066330
10	0.381063		$1.10^4$	0.065363
20	0.300255		2	0.059528
30	0.263463		3	0.056654
40	0.240197		4	0.054776
50	0.223636		5	0.053401
60	0.211018		6	0.052325
70	0.200964		7	0.051448
80	0.192695		8	0.050711
90	0.185731		9	0.050077
$1.10^2$	0.179756		$1.10^5$	0.049523
2	0.146030		2	0.045895
3	0.130328		3	0.044175
4	0.120738		4	0.043020
5	0.114091		5	0.042159
6	0.109125		6	0.041476
7	0.105228		7	0.040913
8	0.102059		8	0.040436
9	0.099413		9	0.040023
$10^3$	0.097158		$10^6$	0.039660

Table 4.8 The Spalding function  $St/\sqrt{C_f/2}$  for  $Pr = 0.7$

$x^+$	$\frac{St}{\sqrt{C_f}/2}$		$x^+$	$\frac{St}{\sqrt{C_f}/2}$
0				
1	0.61424		$1.10^3$	0.07728
2	0.49137		2	0.067892
3	0.43359		3	0.063685
4	0.39639		4	0.061115
5	0.36957		5	0.059300
6	0.34889		6	0.057914
7	0.33224		7	0.056803
8	0.31841		8	0.055880
9	0.30667		9	0.055095
10	0.29650		$1.10^4$	0.054413
20	0.23723		2	0.050335
30	0.20810		3	0.048244
40	0.18965		4	0.046863
50	0.17709		5	0.045843
60	0.16652		6	0.045042
70	0.15856		7	0.044385
80	0.15201		8	0.043830
90	0.14650		9	0.043351
$1.10^2$	0.14177		$1.10^5$	0.042931
2	0.11513		2	0.040295
3	0.10281		3	0.038927
4	0.09510		4	0.038007
5	0.08998		5	0.037319
6	0.08621		6	0.036774
7	0.08327		7	0.036324
8	0.08091		8	0.035943
9	0.07894		9	0.035612
$10^3$	0.07728		$10^6$	0.035321

Table 4.9 The Spalding function  $St/\sqrt{C_f}/2$  for  $Pr = 1$

$x^+$	$\frac{St}{\sqrt{C_f}/2}$		$x^+$	$\frac{St}{\sqrt{C_f}/2}$
0				
1	0.172205		$1.10^3$	0.020749
2	0.137977		2	0.018916
3	0.121054		3	0.018277
4	0.110283		4	0.017932
5	0.102576		5	0.017705
6	0.096672		6	0.017537
7	0.091940		7	0.017406
8	0.088025		8	0.017297
9	0.084709		9	0.017206
10	0.081847		$1.10^4$	0.017127
20	0.064768		2	0.016646
30	0.056777		3	0.016395
40	0.051701		4	0.016225
50	0.048080		5	0.016096
60	0.045315		6	0.015993
70	0.043107		7	0.015907
80	0.041289		8	0.015834
90	0.039754		9	0.015770
			$10^5$	0.015713
$1.10^2$	0.038435			
2	0.030841			
3	0.027396			
4	0.025336			
5	0.023950			
6	0.022950			
7	0.022196			
8	0.021607			
9	0.021135			
$10^3$	0.020749			

Table 4.10 The Spalding function  $St/\sqrt{C_f}/2$  for  $Pr = 7$

$u^+$	$y^+$	$\xi, Pr=0.7$	$\xi, Pr=7.0$	$u^+$	$y^+$	$\xi, Pr=0.7$	$\xi, Pr=7.0$
0	0	0	0	19	219.0	15.90	59.35
1	1	0.7	6.999	20	328.6	16.89	60.36
2	2	1.4	13.99	21	494.6	17.89	61.36
3	3.003	2.101	20.88	22	745.6	18.88	62.37
4	4.013	2.803	27.50	23	1125	19.87	63.37
5	5.042	3.509	33.48	24	1696	20.87	64.37
6	6.115	4.223	38.48	25	2557	21.87	65.38
7	7.274	4.953	42.35	26	3854	22.87	66.38
8	8.590	5.702	45.25	27	5806	23.87	67.38
9	10.18	6.496	47.44	28	8743	24.87	68.38
10	12.23	7.322	49.18	29	13160	25.87	69.38
11	15.04	8.189	50.62	30	19800	26.87	70.38
12	19.06	9.092	51.90	31	29780	27.87	71.38
13	24.98	10.02	53.07	32	44780	28.87	72.38
14	33.88	10.98	54.18	33	67310	29.87	73.38
15	47.36	11.95	55.25	34	101200	30.87	74.38
16	67.88	12.92	56.29	35	152100	31.87	75.38
17	99.13	13.91	57.32	36	228500	32.87	76.38
18	146.7	14.90	58.34	37	343400	33.87	77.38

Table 4.11.  $\xi(y^+, Pr)$  and  $y^+(u^+)$

Note:

(a) For  $Pr = 1$ ,  $\xi = u^+$

(b) For  $y^+ > 300$  the following relations hold:

$$y^+ = 0.3255 \exp. 0.4098 \xi \quad (Pr = 0.7)$$

$$y^+ = 0.09177 \exp. 0.4093 \xi \quad (Pr = 1.0)$$

$$y^+ = 6.317 \times 10^{-9} \exp. 0.4088 \xi \quad (Pr = 7.0)$$

## 5. Description of Apparatus

### 5.1. Introduction

The purpose of this experiment was to obtain an experimental confirmation of the numerical solution that is obtained for an arbitrary heat flux problem. To obtain this an experimental rig was designed in which carbon dioxide was injected into a pipe from a porous wall, the main stream of the pipe being air. The mixed gases were sampled for concentration of carbon dioxide at various stations, and analysed by means of an infra-red gas analyser; the velocity profile in the pipe, just before the injecting section, was fully developed. This was checked by traversing a probe. (Figs. 5.2 and 5.7).

The general layout of the experimental rig is shown in Fig. 5.1 and 5.4. The complete apparatus can be divided into the following five groups:-

1. Air section
2. Diffusing section
3. Test sections
4. CO<sub>2</sub> section
5. Measurements

### 5.2. Air Section

The test rig was on the suction side of an Allis Chalmers compressor with a suction capacity of 3120 cu.ft/min. Air was sucked from the atmosphere, and the air mass flow was controlled by:

1. A control valve on the by-pass line
2. A control valve in the rig after the orifice

Both the control valves were butterfly valves with angular indicators and stop nuts on handle for fixing the valve positions.

The pipe size was made 4.75" internal diameter for the following two reasons:-

1. To facilitate the traverse of the probe for measuring concentration profile very accurately, it was better to have a fairly large size pipe diameter.
2. The final size 4.75" I.D. was decided by the size of the porous tube available.

To obtain a fully developed and an axisymmetric flow, a bell-mouth entry was chosen. The bell-mouth section was made from wood and polished to obtain a very smooth surface.

There is a possibility of asymmetric flow in the pipe if there is the slightest error in coincidence of the axis of the bell-mouth section with that of the main pipe. To prevent this, a straightening grid was inserted immediately after the bell-mouth section. The straightening grid was made by inserting 172 stainless steel tubes, 0.323" O.D., 0.007" thick and 2" long, in a flange 2" thick, 4.75" I.D. (Fig. 5.6).

The gap was filled by a tube separately made to suit the gap. This tube was 0.412" O.D. 0.008" thick and 2" long.

The inlet section was made 22'-6" long and in three pieces, 9 ft., 6ft. and 7ft. -6" respectively. This long length of inlet section, approximately 57 times the internal diameter of the tube, was used to ensure that the air flow just before the test section and the diffusing section, was fully developed turbulent. Further, to obtain a very symmetrical flow, the last piece of inlet section, 7ft. -6" long, and before the diffusing section, was made from perfectly circular drawn tube of one length and 0.125" thick. The other two pieces were made from 16 SWG. 3ft. wide steel sheet.

Between the test section and orifice, a straight pipe 7ft. long was connected in accordance with the British Standards Specification for orifices. (Fig. 5.8).

### 5.3. Diffusing Section

The diffusing section mainly consisted of a porous tube and a diffusing chamber. The porous tube was a high grade ceramic tube with uniform porosity.

The aim of the experiment was to measure the concentration profiles of the diffusing substance at different sections for uniform step mass transfer, followed by a step adiabatic wall. Mass transfer through a porous material depends on three factors:-

1. Static pressure difference
2. Thickness of the porous tube
3. Porosity of the material

Hence to obtain uniform,

1. pressure in the chamber,
2. thickness of the material, and
3. porosity throughout the diffusing length,

the following construction was used:-

1. High grade ceramic tube was used to ensure uniform porosity.
2. The outside and inside surfaces were ground to uniform diameters. During grinding precautions were taken to obtain both the surfaces co-axial and hence of uniform thickness. The manufacturers of the ceramic tube confirmed that grinding does not alter the porosity.
3. The diffusing chamber was made 12" I.D. and 10.25" wide. This large size of chamber gave enough room for the carbon dioxide to settle before it diffused through the porous tube. This, in other words, ensured uniform pressure in the chamber.
4. Carbon dioxide was admitted into the chamber from 16 places, eight on either side of the chamber, equiplaced on 11.125" P.C.D. Two circular ring-mains, made from 0.5" diameter copper tube, supplied carbon dioxide to the chamber at these 16 positions by 0.25" dia. tubes as shown in Fig. 5.5. Carbon dioxide to the ring-mains was supplied from a carbon dioxide cylinder, through the pressure

reducing valve, main valve and the flowmeters.

5. 'O' ring seals were used at all points to prevent any leakages.

#### 5.4. Test Sections

There were two test sections, a small one for measuring the velocity profile and one large one for measuring the concentration profiles. They were made from 4.5" I.D., 0.281" thick mild steel tubes, and they were bored accurately to 4.75" internal diameter. The flanges of these test sections were made to fit in a circular groove of the adjoining flanges so that they could be rotated around the axis of the pipe. With this arrangement, traversing could be made at different circumferential positions to check the axisymmetry of the flow.

The smaller section was mounted before the diffusing chamber. It was made 8" long with only one boss welded in the middle of the length to take the traversing assembly.

The larger section was mounted after the diffusing chamber. It was made 19" long with four bosses welded at four axial positions and at right angles in a consecutive order (see Fig. 5.5).

During the construction of these test sections, all care and precautions were taken to ensure that :-

1. The axes of these test sections were in line with the axis of the main pipe line.
2. No leakages occurred from side surfaces where they rotate. To ensure this 'O' ring seals were used at these surfaces.
3. Traversing axis of the probe was perpendicular to the axis of the pipe and in the same plane.
4. Surfaces of the matching pieces, on which the traversing probe assembly was mounted, were parallel and at a fixed distance from the axis of the pipe.
5. Inside surfaces of the matching pieces on which the traversing probe assembly was mounted, matched the inside curvature of the pipe. To obtain this, test sections were bored accurately to 4.75" I.D., with matching pieces in their position.
6. Inside surfaces was smooth and straight.

#### 5.5. CO<sub>2</sub> Section

CO<sub>2</sub> was obtained from three cylinders (each containing 28 lb of liquid CO<sub>2</sub>) connected in parallel. From these cylinders, CO<sub>2</sub> passed through:-

1. Pressure regulating valve
2. Settling chamber
3. Control valve
4. Two flowmeters, and
5. Orifice

before reaching the diffusing section.  $\frac{1}{8}$ " copper tubes were used for CO<sub>2</sub> pipe line.

At the pressure reducing valve, the temperature of the CO<sub>2</sub> was very low due to its expansion. To bring the temperature of CO<sub>2</sub> back to atmospheric temperature at flowmeter and at diffusing sections, the CO<sub>2</sub> cylinders and pressure reducing valve were placed at a distance from the test rig and the CO<sub>2</sub> cylinders were placed in a water tank. With this arrangement, CO<sub>2</sub> passed through the long length of copper tube (exposed to atmosphere) and in consequence obtained atmospheric temperature before reaching the test rig.

#### 5.6. Measurements

(a) Air mass flow: Air mass flow was measured by an orifice at the downstream side of the test section. The orifice plate was of "D and D/2 taps" type, and it was made according to the British Standard Specification B.S.1042 (1943). To simplify the calculations, the area ratio of orifice to pipe was made 0.5. There were four sets of pressure tapplings at four right angle circumferential positions. Pressure differences across the orifice were measured on vertical water manometers. The mean of these four sets of pressure differences was used to obtain air mass flow.

(b) CO<sub>2</sub> flow: The flow of CO<sub>2</sub> was measured by two Fischer & Porter percentage type flowmeters. They read accurately within  $\pm 2\%$  of the maximum flow. Two flowmeters were used in series to cover the wide range of CO<sub>2</sub> flow. 100% reading on the small flowmeter represented 0.97 cu.ft./min. at 14.7 p.s.i. and 60°F., and 100% reading on large flowmeter represented 3.72 cu.ft./min. at 14.7 p.s.i. and 70°F. For different temperature and pressure conditions, the flow was corrected by the use of curves supplied by the manufacturers.

At first it was found that the amount of CO<sub>2</sub> flowing through the pipe and measured by the gas analyser was less than the CO<sub>2</sub> measured by the flowmeter. After checking leaks in the CO<sub>2</sub> line, the flowmeters were suspected. For an approximate check on flowmeters, an orifice was introduced in the CO<sub>2</sub> pipe line, and this confirmed the accuracy of the flowmeters (see Figs. 7.3 and 7.4). Later on the fault was found in the sampling cell of the infra-red gas analyser. The cell was cracked and, in consequence, air was leaking into the cell resulting in low concentration measurements. The cell was then replaced by a new one.

(c) Concentration of CO<sub>2</sub>: Concentration of CO<sub>2</sub> was measured by an infra-red gas analyser type S.B.1. This gas analyser has two absorbing lengths. One length is a standard cell, whereas the other length has two cells, one for pure air and another for the sample to be tested. Radiation from the nichrome heaters passes through the absorption tubes and thence two two receivers, which are filled with the gas to be detected. These receivers are partitioned off from one another by a thin metal diaphragm, and form an electric condenser. Absorption of infra-red radiation in the sampling cell depends on the concentration of carbon dioxide.

This absorption of radiation causes a pressure difference between the two receiving chambers, with the result that the thin diaphragm deforms and causes a variation of the capacity. The resulting capacity changes are amplified electronically and a final indication is obtained on an output galvanometer.

The sampling length was on the suction side of a Charles Austen Mk. 1 pump with a capacity of 3500 c.c./min. The amount of suction was adjusted by controlling

the speed and the opening on the by-pass line. The sample from the traversing probe was passed through the drying tube and filter before passing through the sampling cell. Pure air was passed through the drying tube and a tube containing soda asbestos to remove carbon dioxide before it entered the standard cell (Fig. 5.3). Moisture was removed from the sample because it absorbs the infra-red radiation of the same wavelength as carbon dioxide and would give a false reading. Thin (1/8" O.D.) polythene tubing was used for connections.

The gas analyser was calibrated for two ranges of concentration, and the calibration curves are shown in Figs. 7.1 and 7.2. Calibration was done by mixing a known amount of carbon dioxide with a known amount of air, and measuring the galvanometer reading for the mixture. The flow of carbon dioxide was measured by a soap-bubble flowmeter and airflow was measured by a gasmeter.

During calibration a standard bottle was made in which carbon dioxide was mixed with air, and the galvanometer reading for that mixture was measured. The instrument was also provided with a calibration system consisting of a metallic wire which comes between the sampling cell and a receiving chamber (when operated by a solenoid switch) and absorbs a fixed amount of radiation giving a standard galvanometer reading.

During tests, the same conditions and suction were used as during calibration, the instrument being frequently checked by the "wire" reading and the standard bottle for the same galvanometer readings.

(d) Pressure measurement: To obtain the friction factor in the pipe, the static pressure gradient for a fixed length of pipe was measured on a Betz manometer. This length was selected where the flow was fully developed (after a length of 40 diameters from entry). The velocity profile was measured by measuring the static pressure on a vertical water manometer and the difference of pressure between the total and static on a Betz manometer. The pitot tube was traversed at the test section before the diffusing chamber.

## 6. Test Procedure - Calculation Procedure

### 6.1. Introduction

The aim of this experimental investigation was to obtain an experimental confirmation of the numerical solution. The test rig was made in which carbon dioxide was injected through a porous section of the tube wall, while air was flowing turbulently in the axial direction. The injecting length was 10.25" and the concentration profiles in the boundary layer were measured downstream of the injection section. The injection was assumed to be uniform. Conditions are therefore such that the concentration profiles are measured for a step length of uniform injection followed by an impermeable wall. In heat transfer, this is a problem of finding temperature profiles for step heat flux followed by an adiabatic wall. The flow in the pipe was fully developed and wall shear stress, therefore, was uniform in the test section.

### 6.2. Procedure of Test

The test procedure was very simple. It involved traversing a probe and measuring the galvanometer reading, which in consequence gave, directly from

the calibration curves, the concentration of the carbon-dioxide at that particular position. A test card (Fig. 6.0) is attached to explain the measurements taken during the test. Each test took approximately two days to run, and comprised:

1. Three to and fro traverses for concentration profiles at the axial section but at three circumferential positions called positions A, B, and C.
2. Velocity traverse before the diffusing section.

During the test, the main stream air flow and the flow of carbon dioxide were kept constant. All possible precautions were taken to obtain true readings, e.g.

1. Giving enough time for the galvanometer reading to settle
2. Checking drying agents
3. Checking very often the wire reading of the I. R. G. A.
4. Checking air flow and carbon dioxide flow, etc.

Before starting the actual profile tests, many preliminary tests were carried out to ensure that all the measurements were correct and reliable.

#### 6.3. Preliminary tests

To confirm that the flow was fully turbulent, the velocity profiles for various main stream velocities were measured at the test section before the diffusing section. The results were found to lie on a plot of Universal Velocity Profile (Fig. 7.5). Velocity profiles obtained were integrated to check the air mass flows, and were found to agree within 2% with the mass flows obtained from the orifice meter. Simultaneously, ratios of average to maximum velocities were calculated and compared with the previous investigators. The results were found to be satisfactory (Fig. 7.8).

The knowledge of the friction factor was necessary for the theoretical calculation of the concentration profile. Instead of using the well known equation of Von Karman etc. for the calculation of the friction factor, it was decided to measure the actual friction factor and use this experimental value for the theoretical calculation. The friction factor was obtained by measuring the pressure drop in the pipe, across a length of 57", on the Betz manometer. The results are shown in Fig. 7.9. The best fit curve through the experimental points was found to be

$$C_f/2 = 0.04135 (\text{Red})^{-0.254} \quad (6.1)$$

The gas analyser was calibrated for two ranges of concentration 0. to 1.1% and 0 to 2.9%. To prevent any error, the calibrations were carried out in the conditions that would occur during the concentration profile test. Calibration was carried out by the method indicated earlier.

To measure the flow of carbon dioxide, two flowmeters were used in series to cover a wide range. These flowmeters were compared with each other in the intermediate region of flows for which both gave indications (Fig. 7.3). Simultaneously, an orifice was included in the line to check the flow measured by

the flowmeter. The orifice was not made according to the British Standard Specification which limits to the orifice diameter of 0.5". In this instance the diameter of the orifice was 0.25" with  $m = 0.346$ . For such a small diameter the correction factor was very high and was out of the region given in B.S.1042. The flowmeter therefore was compared with the orifice meter without applying the correction factor to the orifice readings. The error in the orifice meter was therefore expected to be in the region of 10 to 15%. Comparison is shown in Fig. 7.4.

It is known that the concentration at any point in the boundary layer is directly proportional to the injection rate. To check that the measurements are reliable, a quick test was carried out in which the concentrations were measured at a fixed position in the boundary layer for various injection rates. The test was carried out for two different main stream velocities. The results confirmed the reliability of the measurements (Fig. 7.7.).

#### 6.4. Calculation Procedure (Experimental)

The concentration of the injected carbon dioxide for a given galvanometer reading was obtained directly from the calibration curves. For each test there were three sets of measurements for concentration profile at three circumferential positions, and a mean curve through these three sets of results was considered as a concentration profile at that particular section for that particular main stream velocity and injection rate.

The average velocity of air through the pipe was calculated from

$$\bar{u} = 4.685 Z \sqrt{\frac{h T_s}{P_s}} \quad (6.2)$$

$h = h_s - h_o$  = pressure differential across the orifice in inches of water

$T_s$  = temperature of air at upstream of the orifice in  $^{\circ}\text{K}$ .

$P_s$  = pressure upstream of the orifice in  $\text{lb./in}^2$ .

$Z$  = correction factor from B.S.1042.

Reynolds number was obtained from

$$\text{Red} = \frac{\bar{u} D}{\nu} = \frac{\bar{u} \times 4.75}{12 \nu} \quad (6.3)$$

Flow of carbon dioxide  $\dot{V}$  in  $\text{cu.ft./sec.}$  was obtained by multiplying the percentage reading on the flowmeter with a constant factor. 100 per cent reading on the large flowmeter represented 0.062  $\text{cu.ft./sec.}$  at 14.7 p.s.i. and  $70^{\circ}\text{F}$ . and 100 percent reading on the small flowmeter represented 0.0162  $\text{cu.ft./sec.}$  at 14.7 p.s.i. and  $70^{\circ}\text{F}$ . Correction factors for temperature and pressure were obtained from the curves supplied by the manufacturers. The injecting surface area of the porous tube was  $1.062 \text{ ft}^2$ .

$$\therefore \dot{V}_w'' = \frac{\dot{V}}{1.062} \text{ cu.ft./sec.ft}^2 \quad (6.4)$$

To compare the experimental concentration profiles with the theoretical

concentration profiles, the readings of the concentration profiles were multiplied by a factor  $\frac{\bar{u}}{100 \dot{V}_w}$ . In other words, all the concentration profiles were for a ratio of injection velocity to main stream velocity = 1/100.

The velocity profile in the boundary layer was obtained by traversing a probe and using

$$u = 14.93 \sqrt{\frac{h T_2}{P_2}} \quad (6.5)$$

where  $h = h_3 - h_2 =$  total pressure - static pressure in inches of water  
 $T_2 =$  temperature in  $^{\circ}\text{K}$   
 $P_2 =$  Pressure in  $\text{lb./in}^2$ .

During the friction factor test, the friction factor was calculated from

$$\frac{\tau_w}{g} \times \pi D L = (P_1 - P_2) \frac{\pi}{4} D^2 \quad (6.6)$$

i.e.

$$C_f/2 = \frac{g(P_1 - P_2)}{\rho \bar{u}^2} \times \frac{D}{4L} \quad (6.7)$$

$L =$  length of pipe in ft.

$D =$  diameter of the pipe in ft.

$(P_1 - P_2) =$  pressure loss in  $\text{lb./ft}^2$ .

#### 6.5. Calculation Procedure (Theoretical)

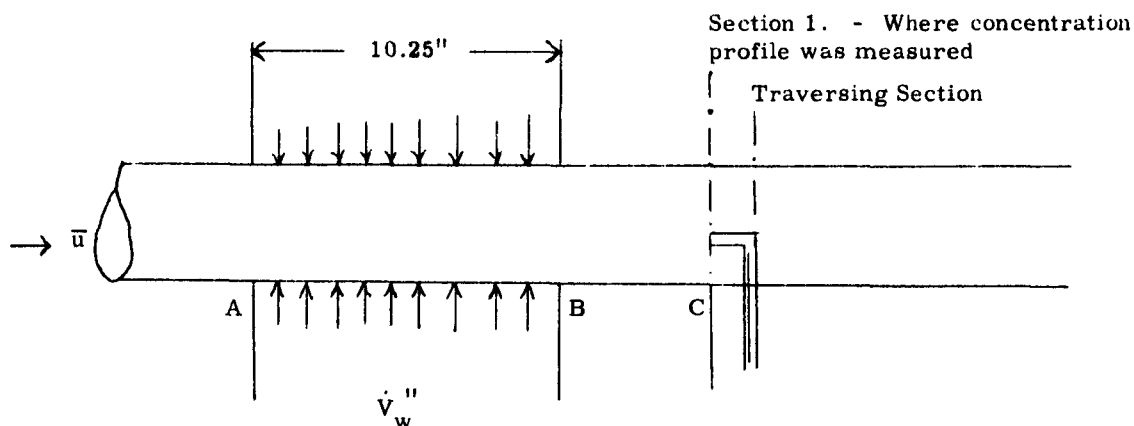


Fig. 6.1

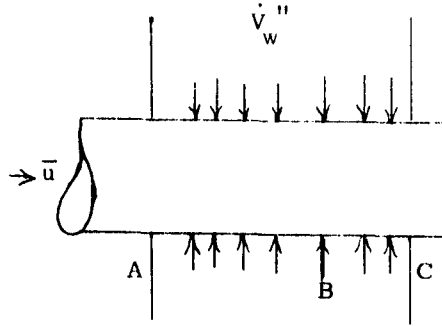


Fig. 6.2

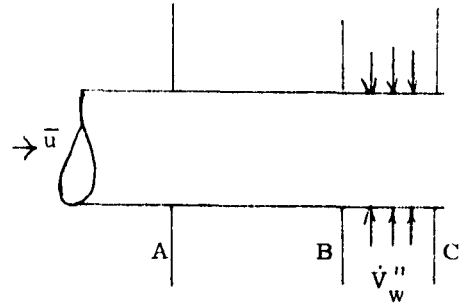


Fig. 6.3

In the experimental rig, the injection was assumed to be uniform and therefore this was a case of step heat flux followed by an adiabatic wall (Fig. 6.1). To apply the numerical solution for step heat flux, this problem was considered in two steps:

1. Solution for uniform injection from A to C (Fig. 6.2)
2. Solution for uniform injection from B to C (Fig. 6.3)

The final solution was obtained by subtracting the second solution from the first. For carbon dioxide diffusing in air, the Schmidt number is 0.91, and therefore the numerical solution for  $Pr = 1$  was used to obtain the theoretical concentration profile.

The calculation of the theoretical concentration profile can be summarised as follows:-

1. Calculation of  $x_1^+$  and  $x_2^+$  from

$$x^+ = \sqrt{C_f/2} \times Red \times \frac{L}{D} \quad (6.8)$$

$L$  = injecting length.

$\bar{u}$  and  $Red$  are known from the experimental calculation. Friction factor  $C_f/2$  is obtained from the experimental relation:

$$C_f/2 = 0.04135 (Red)^{-0.254} \quad (6.9)$$

(2) Reading the values of Spalding functions:

$$\left( \frac{St_m}{\sqrt{C_f/2}} \right)_1, \text{ and } \left( \frac{St_m}{\sqrt{C_f/2}} \right)_2 \text{ for } x_1^+ \text{ and } x_2^+ \text{ from Fig. 4.4.}$$

(3) Knowing  $\sqrt{C_f/2}$ ,  $(St_m)_1$  and  $(St_m)_2$  are obtained from (2).

$$St_m = \frac{\dot{V}_w''}{C_w \bar{u}} = \text{Equivalent of Stanton number in mass transfer}^*$$

$\dot{V}_w''$  = injection rate in cu.ft./sec.ft.<sup>2</sup>.

$\bar{u}$  = average velocity ft./sec.

$C_w$  = surface concentration of the carbon dioxide in cu.ft./cu.ft. of mixture.

(4) Theoretical solution was carried out for  $\frac{\dot{V}_w''}{\bar{u}} = 1/100$ . Hence  $C_{w1}$  and  $C_{w2}$  are calculated from (3).

(5) For Schmidt number equal to 1, the concentration profiles are given in Fig. 4, in the form of  $C/C_w$  for a large range of  $x^+$ . Knowing  $C_{w1}$  and  $C_{w2}$ , the concentration profiles for  $x_1^+$  and  $x_2^+$  are obtained.

(6) The final theoretical concentration profile is obtained by subtracting the concentration profile for  $x_2^+$  from the concentration profile of  $x_1^+$ .

(7) The concentration profile obtained above is in the form of  $C(\xi)$  and not  $C(y)$ . From Fig. 4.8 and

$$y^+ = \frac{y}{D} \frac{\bar{u}D}{\nu} \sqrt{C_f/2} \quad (6.10)$$

$C(y)$  can be obtained.

---

\* Note that this definition is identical with  $St_m = \frac{\dot{m}_w''}{\rho_w \bar{u}}$  where  $\dot{m}_w''$  is the mass rate of flow of carbon dioxide per unit area at the wall, and  $\rho_w$  is the true density of carbon dioxide at the wall (i.e. mass/unit volume of space).

## 7. Results and Conclusions

### 7.1. Results

The results of the preliminary tests and eight concentration profile tests are shown in fourteen tables (Tables 7.1 to 7.14) and 21 graphs (Figs. 7.1 to 7.21).

Tables 7.1 to 7.8 contain the measurements of eight concentration profile tests. Table 7.9 contains the summary of the eight tests. Measurements for the calibration of the I. R. G. A. are shown in Tables 7.10 and 7.11. Table 7.12 shows the measurements of friction factor, and Tables 7.13 and 7.14 show the comparison of the flowmeters for  $\text{CO}_2$ .

The calibration of the I. R. G. A. is shown in Figs. 7.1 and 7.2. Figs. 7.3 and 7.4 show comparison of flowmeters for carbon dioxide. Measurement of the velocity profile is shown in Fig. 7.5, and comparison with Spalding's velocity profile is given in Fig. 7.6. The results of the friction factor measurements are shown in Fig. 7.9. In Fig. 7.8, the ratio of the average to maximum velocity is compared with the results of the previous investigators. The results of the test confirming the direct variation of the concentration with the injection rate is given in Fig. 7.7. In Fig. 7.10, the theoretical concentration profile at section 1 is shown for various main stream velocities.

Figs. 7.11 to 7.18 show the experimental concentration profiles of the eight tests. Fig. 7.19 show the concentration profiles for tests 5 to 8, in which the main stream velocity was fixed but the injection rate was varied. Fig. 7.20 gives the concentration profiles of tests 5 to 8 (converted for fixed  $V_w''$ ) confirming the linearity of the concentration with the injection rate. Finally, Fig. 7.21 shows the comparison of the experimental concentration profiles with the theoretical profiles.

### 7.2. Conclusions

On the theoretical side, the problem of heat and mass transfer from non-isothermal surfaces has been attacked in two ways.

1. Approximate solutions are obtained for laminar and turbulent cases, by assuming the shape of velocity and temperature profiles in the boundary layer and integrating the energy equation. The equations obtained are very simple and predict results that are in agreement with those of Rubesin<sup>(15)</sup>, and Reynolds et al<sup>(10)</sup>.
2. Exact solution of the partial differential equation is obtained for a step heat flux problem and for Prandtl numbers 0.7, 1 and 7. The numerical integration was carried out on a Digital Computer. Spalding's Velocity Law was used with an assumption of unity turbulent Prandtl number. A method has been developed to apply this solution to an arbitrary heat flux problem. Various methods are known to exist in which the heat transfer coefficient can be calculated for an arbitrary heat flux case. But so far as the authors know, the method presented in this report is the only method that exists in which, in addition to the calculations of heat transfer at the surface, the temperature within the boundary layer can be calculated. Due to lack of time, it has not been possible to compare these solutions with the experimental results of Reynolds et al<sup>(10)</sup>.

$y''$	Concentration in cu. ft./100 cu. ft.	Concentration in cu. ft./100 cu. ft. for $\frac{y''}{w} = \frac{1}{100}$	$u$ ft./sec.
0	1.135	52.5	0
0.01	1.128	52.2	33.5
0.02	1.115	51.6	41.3
0.04	1.085	50.2	47
0.06	1.05	48.6	50.2
0.08	1.005	46.5	52.5
0.1	0.95	44	54.3
0.15	0.81	37.5	57.2
0.2	0.65	30.1	59.3
0.25	0.513	23.75	61
0.3	0.4	18.53	62.5
0.4	0.22	10.2	64.6
0.5	0.113	5.23	66
0.6	0.06	2.78	67.3
0.7	0.03	1.39	68.5
0.8	0.013	0.6015	69.5
0.9	0.01	0.463	70.3
1	0.005	0.231	71

$y''$	Concentration in cu. ft./100 cu. ft.	Concentration in cu. ft./100 cu. ft. for $\frac{y''}{w} = \frac{1}{100}$	$u$ ft./sec.
0	2.08	49.75	0
0.01	2.06	49.25	48.5
0.02	2.04	48.8	56.6
0.04	1.98	47.35	63.6
0.06	1.905	45.5	67.8
0.08	1.815	43.4	70.6
0.1	1.74	41.65	73
0.15	1.487	35.55	76.5
0.2	1.235	29.53	79.3
0.25	1	23.9	81.7
0.3	0.79	18.9	83.1
0.4	0.453	10.83	86.1
0.5	0.227	5.43	88
0.6	0.115	2.75	89.8
0.7	0.067	1.6	91.3
0.8	0.033	0.789	92.6
0.9	0.02	0.478	93.8
1	0.01	0.239	94.8

TABLE 7.1. RESULTS OF TEST 1

TABLE 7.2. RESULTS OF TEST 2

$y''$	Concentration in cu.ft/100 cu.ft.	Concentration in cu.ft/100 cu.ft. $\frac{v''}{w} = \frac{1}{u}$	$u$ ft/sec.
0	0.855	50	0
0.01	0.846	49.5	56
0.02	0.836	48.9	66.5
0.04	0.817	47.8	74
0.06	0.786	46	79.2
0.08	0.752	44	82.3
0.1	0.711	41.6	84.7
0.15	0.581	34	89
0.2	0.463	27.1	92.25
0.25	0.363	21.25	94.7
0.3	0.274	16.05	96.5
0.4	0.144	8.42	99.75
0.5	0.07	4.1	102.2
0.6	0.03	1.755	104.1
0.7	0.005	0.293	105.8
0.8	-	-	107.2
0.9	-	-	108.7
1	-	-	110

$y''$	Concentration in cu.ft/100 cu.ft.	Concentration in cu.ft/100 cu.ft. $\frac{v''}{w} = \frac{1}{u}$	$u$ ft/sec.
0	0.806	48.3	0
0.01	0.803	48.2	60
0.02	0.797	47.85	70.5
0.04	0.783	47	79.5
0.06	0.766	46	84.5
0.08	0.739	44.35	87.5
0.1	0.701	42.1	90.2
0.15	0.579	34.75	95
0.2	0.463	27.8	98
0.25	0.36	21.6	100.7
0.3	0.265	15.9	102.8
0.4	0.138	8.28	106
0.5	0.068	4.08	108.5
0.6	0.035	2.1	110.7
0.7	0.016	0.96	113.3
0.8	0.006	0.36	116
0.9	0.002	0.12	118
1	-	-	120

TABLE 7.3. RESULTS OF TEST 3

TABLE 7.4. RESULTS OF TEST 4

y"	Concentration in cu. ft/100 cu. ft.	Concentration in cu. ft/100 cu. ft. for $\frac{\dot{v}''}{\bar{w}} = \frac{1}{100}$	u ft/sec.
0	2.11	48.8	0
0.01	2.10	48.3	43
0.02	2.086	48.2	50
0.04	2.045	47.2	57
0.06	1.98	45.8	60.5
0.08	1.9	43.9	63.2
0.1	1.787	41.3	65.3
0.15	1.515	35	68.8
0.2	1.26	29.1	71.25
0.25	1.027	23.85	73.1
0.3	0.817	18.9	74.7
0.4	0.485	11.2	77.2
0.5	0.255	5.89	79.15
0.6	0.13	3	80.7
0.7	0.05	1.155	82
0.8	0.03	0.693	83.1
0.9	0.015	0.347	84.1
1	0.01	0.23	85

TABLE 7.6. RESULTS OF TEST 6

y"	Concentration in cu. ft/100 cu. ft.	Concentration in cu. ft/100 cu. ft. for $\frac{\dot{v}''}{\bar{w}} = \frac{1}{100}$	u ft/sec.
0	2.535	50.15	0
0.01	2.525	50	43
0.02	2.5	49.4	50
0.04	2.443	48.3	57
0.06	2.37	46.85	60.5
0.08	2.285	45.1	63.2
0.1	2.175	43	65.3
0.15	1.86	36.8	68.8
0.2	1.553	30.7	71.25
0.25	1.255	24.8	73.1
0.3	0.99	19.57	74.7
0.4	0.58	11.47	77.2
0.5	0.313	6.19	79.15
0.6	0.166	3.28	80.7
0.7	0.09	1.78	82
0.8	0.047	0.93	83.1
0.9	0.02	0.395	84.1
1	0.01	0.198	85

TABLE 7.5. RESULTS OF TEST 5

y"	Concentration in cu. ft./100 cu. ft.	Concentration in cu. ft./100 cu. ft. for $\frac{\dot{v}''}{w} = \frac{1}{100}$	u ft./sec.
0	1.485	51.4	0
0.01	1.480	51.2	43
0.02	1.465	50.7	50
0.04	1.42	49.2	57
0.06	1.367	47.3	60.5
0.08	1.308	45.25	63.2
0.1	1.237	42.8	65.3
0.15	1.063	36.8	68.8
0.2	0.883	30.5	71.25
0.25	0.713	24.65	73.1
0.3	0.553	19.1	74.7
0.4	0.3	10.38	77.2
0.5	0.165	5.71	79.15
0.6	0.088	3.05	80.7
0.7	0.047	1.625	82
0.8	0.02	0.692	83.1
0.9	0.01	0.346	84.1
1	0.005	0.173	85

TABLE 7.7. RESULTS OF TEST 7

y"	Concentration in cu. ft./100 cu. ft.	Concentration in cu. ft./100 cu. ft. for $\frac{\dot{v}''}{w} = \frac{1}{100}$	u ft./sec.
0	0.913	50.6	0
0.01	0.905	50.25	43
0.02	0.897	49.7	50
0.04	0.875	48.5	57
0.06	0.845	46.8	60.5
0.08	0.81	44.9	63.2
0.1	0.77	42.6	65.3
0.15	0.653	36.2	68.8
0.2	0.54	29.9	71.25
0.25	0.43	23.85	73.1
0.3	0.333	18.45	74.7
0.4	0.195	10.8	77.2
0.5	0.11	6.1	79.15
0.6	0.06	3.32	80.7
0.7	0.03	1.663	82
0.8	0.02	1.11	83.1
0.9	0.01	0.555	84.1
1	0.005	0.277	85

TABLE 7.8. RESULTS OF TEST 8

Test No.	$\bar{u}$ ft/sec.	Red $\times 10^{-5}$	$C_f/2$	Flowmeter Reading	Flow of CO <sub>2</sub> in cu. ft/mt	$\dot{v}_w''$ ft/sec.	Integrated $\dot{v}_w''$ ft/sec.	Percentage difference
1	67.6	1.632	0.001963	95 x	0.93	0.0146	0.01475	1.02%
2	90.9	2.221	0.00182	65 *	2.415	0.038	0.0376	1.055%
3	105.2	2.695	0.00177	29 *	1.08	0.01795	0.01655	7.81%
4	112.9	2.726	0.00173	30 *	1.116	0.0182	0.01704	6.37%
5	80.85	1.964	0.00189	70 *	2.61	0.0409	0.0425	3.77%
6	80.85	1.964	0.00189	60 *	2.23	0.035	0.0348	0.571%
7	80.85	1.964	0.00189	40 *	1.488	0.02335	0.02387	2.18%
8	80.85	1.964	0.00189	95 x	0.93	0.0146	0.01487	1.41%

TABLE 7.9. RESULTS OF THE EIGHT TESTS

\* Large Flowmeter

x Small Flowmeter

No.	Time in Secs. for 25 c. c. of CO <sub>2</sub>	Time in Secs. for 5000 c. c. of Air	CO <sub>2</sub> flow in c. c. /mt.	Air flow in c. c. /mt.	Total flow in c. c. /mt.	Concentration of CO <sub>2</sub> in c. c. /100 c. c.	Galvanometer Reading
1	299	265	5.02	1133	1138	0.441	44
2	543	251.6	2.765	1192	1195	0.2313	24
3	737	249	2.035	1206	1208	0.1685	20
4	39.7	86.4	37.8	3473	3511	1.077	99
5	43.8	89.2	34.25	3367	3401	1.003	92
6	69.8	89.2	21.5	3360	3381	0.636	60
7	77.3	88.8	19.43	3375	3394	0.573	54.5
8	96.6	89.4	15.54	3353	3368	0.462	45
9	139	86.5	10.79	3470	3481	0.31	31.5
10	164.6	85.7	9.12	3500	3509	0.26	27
11	244.5	86.4	6.135	3470	3476	0.1765	19
12	319.5	87	4.69	3450	3455	0.1362	17
13	211	92.6	7.09	3240	3247	0.2186	22
14	273.5	91.4	5.48	3285	3290	0.1667	17.5
15	547	93	2.745	3227	3230	0.085	9
16	130	99.35	11.54	3020	3031	0.381	36
17	90.2	92.4	16.63	3246	3262	0.51	50
18	51.8	94.4	28.95	3175	3205	0.904	85.5
19	43.8	92.2	34.25	3255	3290	1.04	96
20	79.2	89.4	18.93	3360	3379	0.56	53.5
			etc.				

TABLE 7.10. CALIBRATION OF I. R. G. A. (Range 0 - 1.1%)

No.	Time in Secs. for 100 c.c. of CO <sub>2</sub>	Time in Secs. for 10000 c.c. of Air	CO <sub>2</sub> flow in c.c./mt.	Air flow in c.c./mt.	Total flow in c.c./mt.	Concentration of CO <sub>2</sub> in c.c./100 c.c.	Galvanometer Reading
1	105.4	160	56.9	3750	3907	1.494	55.75
2	120.4	160.4	49.85	3750	3900	1.312	49
3	163.2	158	36.8	3900	3936	0.959	38
4	61.5	163.2	97.6	3675	3772	2.588	86
5	66.2	159.3	90.6	3765	3855	2.35	85
6	89.8	162	66.8	3710	3777	1.769	66
7	129.5	164	46.3	3660	3716	1.245	48
8	193.4	163	31	3675	3706	0.836	32.5
9	307	162.6	19.54	3690	3710	0.527	20
10	385.6	163.7	15.57	3670	3686	0.422	17.75
11	411	163.2	14.6	3670	3685	0.396	16.25
12	57	162.5	105.2	3710	3915	2.83	98.75
13	61.8	162	97.15	3710	3907	2.555	91.25
14	288	160	20.85	3750	3771	0.553	22.5
15	606	159.7	9.9	3750	3770	0.262	9.5
16	83.15	159.2	72.2	3760	3832	1.94	70.5
17	76.7	158.8	78.15	3780	3858	2.027	75.75
18	243.2	151.5	24.67	3960	3985	0.62	25.25
19	92.7	155	64.7	3870	3935	1.645	59.5
20	112.7	155	53.3	3870	3923	1.359	47.25
				etc.			

TABLE 7.11. CALIBRATION OF I. R. G. A. (Range 0 - 2.9%)

No.	$\bar{u}$ ft/sec.	$\rho$ lbs/cu. ft.	Red $\times 10^{-5}$	$h_f$ in m. m.	$C_{f/2}$
1	87.7	0.0753	2.205	7.735	0.001827
2	82.4	0.0754	2.073	6.85	0.001827
3	78.1	0.0755	1.963	6.26	0.001855
4	92.1	0.0752	2.314	8.4	0.0018
5	118.9	0.07435	2.99	13.1	0.001707
6	114.7	0.07445	2.882	12.135	0.001692
7	110.4	0.0746	2.777	11.325	0.001705
8	146.5	0.07335	3.685	18.4	0.001596
9	139.7	0.0736	3.51	16.85	0.001606
10	134.7	0.0738	3.387	15.875	0.001618
11	127.9	0.074	3.22	14.5	0.00164
12	102.8	0.0748	2.587	9.85	0.001705
13	73.35	0.0756	1.844	5.2	0.00175
14	60.3	0.0758	1.517	3.975	0.001974
15	49.4	0.076	1.243	2.84	0.002092
16	34.9	0.0762	0.8775	1.58	0.00232
17	24	0.07625	0.6035	0.86	0.002675

TABLE 7.12. FRICTION FACTOR MEASUREMENTS

$$C_{f/2} = \frac{g(p_1 - p_2)}{\rho \bar{u}^2} \frac{D}{4L}$$

$$L = 57''$$

$$D = 4.75''$$

No.	Reading on small flowmeter	Reading on large flowmeter	Flow in cu. ft/mt. small flowmeter	Flow in cu. ft/m large flowmeter
1	93	24.6	0.911	0.915
2	96	25.4	0.941	0.944
3	90	23.8	0.882	0.885
4	83.7	22.2	0.82	0.826
5	81	21.6	0.7935	0.8035
6	75	19.8	0.735	0.7365
7	59.5	15.3	0.583	0.569
8	97	25.5	0.95	0.948
9	89	23.4	0.872	0.87
10	87	23	0.852	0.856
11	73	19.2	0.715	0.714
12	82	21.8	0.803	0.811
13	82.5	22	0.808	0.8185
14	79	20.85	0.7735	0.775
15	74.6	19.5	0.730	0.725
16	68	17.9	0.660	0.666
17	85	22.4	0.833	0.833

TABLE 7.13. COMPARISON OF FLOWMETERS

100 percent reading on small flowmeter represents  
0.98 cu. ft/mt at 14.7 p.s.i. and 70°F.

100 percent reading on large flowmeter represents  
3.72 cu. ft/mt at 14.7 p.s.i. and 70°F.

No.	Reading on large flowmeter	Flow in cu. ft./mt. (flowmeter)	Pressure difference across the orifice in m. m.	Flow in cu. ft./mt. (orifice)	Percentage difference
1	20	0.744	22.25	0.671	11%
2	25	0.93	34.77	0.839	11%
3	30	1.116	49.2	0.998	11.7%
4	35	1.302	66.65	1.162	12.1%
5	40	1.488	86.77	1.326	12.3%
6	45	1.674	109.5	1.488	12.5%
7	50	1.86	134.7	1.65	12.7%
8	55	2.045	162.3	1.813	12.7%

TABLE 7.14. COMPARISON OF FLOWMETER WITH ORIFICEMETER

The experiment was started with the idea of obtaining an experimental confirmation of the numerical solution. It was, therefore, planned to measure the concentration profiles at :-

1. Various sections downstream of the injection for various,
2. mainstream velocities,
3. injection rates,
4. injecting lengths.

Eight tests were carried out in which concentration profiles were measured at section 1 for a few main stream velocities and injection rates.

Comparison of the experimental results with the theoretical solution is shown in Fig. 7.20 and Fig. 7.21. It is seen from this comparison that :-

- (1) Experimental results show higher diffusion of  $\text{CO}_2$  in the boundary layer than that of the theoretical solution, and in consequence:
- (2) the measured surface concentration is lower than that of the theoretical solution.
- (3) The shape of the measured concentration profile is different from that of the theoretical solution.

There is no doubt about the accuracy of the experimental results because:-

1. The amount of carbon dioxide obtained by integrating the concentration profile agreed with the amount of carbon dioxide injected through the porous tube.
2. The concentration at any point varied directly with the injection rate.
3. The shape of the concentration profile did not vary with the injection rate.
4. All the eight tests consistently showed a similar shape of the concentration profile in the boundary layer.

The authors feel that the disagreement with the theoretical solution are due to the following reasons:-

- (1) The theoretical concentration profiles for comparison with the experimental results were obtained on the assumption that the injection through the porous tube is uniform throughout the injecting length. There is no experimental confirmation to this assumption.
- (2) The theoretical solution is for two dimensional flow, and measurement of higher diffusion may be due to reduction in cross-sectional area (due to decrease in radius) with increase in  $y$  (distance from surface).

8. References

1. Seban, R. A. Calculation method for two dimensional laminar boundary layers with arbitrary free stream velocity variation.  
University of California, Inst. of Eng. Res. Report 2-12, 1950.
2. Seban, R. A. ,  
Chan, H. W. Heat transfer to boundary layers with pressure gradients.  
WADC TR 57-111, ASTIA, Document No. AD.118075, 1958.
3. Drake, R. M. Calculation method for three-dimensional rotationally symmetrical laminar boundary layers with arbitrary free-stream velocity and arbitrary wall-temperature variation.  
J. Aero.Sci. , Vol. 20, 1953, pp 309-316.
4. Schuh, H. A new method for calculating laminar heat transfer on a cylinder of arbitrary cross section and on bodies of revolution at constant and variable wall temperature.  
K. T. H. Aero. TN.33, Stockholm, 1953.
5. Lighthill, M. J. Contributions to the theory of heat transfer through a laminar boundary layer.  
Proc. Roy. Soc. A, Vol. 202, 1950, pp 359-377.
6. Tribus, M. ,  
Klein, J. Forced convection through a laminar boundary layer over an arbitrary surface with an arbitrary temperature variation.  
J. Aero.Sci. , Vol. 22, 1955, pp 62-64.
7. Ambrok, G. S. Approximate solution of equations for the thermal boundary layer with variations in boundary layer structure.  
Soviet Physics, Vol. 2, 1957, pp 1979-1986.
8. Spalding, D. B. Heat transfer from surfaces of non-uniform temperature.  
J. Fluid Mech. , Vol. 4, 1958, pp 22-32.
9. Eckert, E. R. G. ,  
Drake, R. M. Heat and mass transfer.  
McGraw-Hill Book Co. , Inc. , New York, 1959.
10. Reynolds, W. C. ,  
Kays, W. M. ,  
Kline, S. J. Heat transfer in the turbulent incompressible boundary layer. III. Arbitrary wall temperature and heat flux.  
NASA Memo. 12-3-58W, 1958.
11. Rubesin, M. W. The effect of an arbitrary surface-temperature variation along a flat plate on the convective heat transfer in an incompressible turbulent boundary layer.  
NACA TN. 2345, 1951.

References (Continued)

12. Seban, R. Theory reported in Scessa, S. Experimental investigation of convective heat transfer to air from a flat plate with a stepwise discontinuous surface temperature.  
M.S. Thesis, Univ. of California, Berkeley, 1951.
13. Schlichting, M. Boundary layer theory.  
Pergamon Press, London 1955.
14. Maisel, D. S. ,  
Sherwood, T. K. Evaporation of liquids into turbulent gas streams.  
Chem. Engng. Prog. , Vol. 131, 1950.
15. Rubesin, M. W. An analytical investigation of the heat transfer between a fluid and a flat plate parallel to the direction of flow having a stepwise discontinuous surface temperature.  
M.S. Thesis, Univ. of California, Berkeley, 1945.
16. Spalding, D. B. Heat transfer to a turbulent stream from a surface with a stepwise discontinuity in wall temperature.  
Int. Developments in Heat Transfer, Part II, p. 439. A. S. M. E., 1961.
17. Muralidharan, R. Work referred to in Ref. 16.
18. Kestin, J. ,  
Persen, L. N. Application of Schmidt's method to the calculation of Spalding's function and of the skin-friction coefficient in turbulent flow.  
Int. J. Heat Mass Transfer, Vol. 5, 1962, pp 143-151.
19. Bond, R. Heat transfer to a laminar boundary layer with non-uniform free stream velocity and non-uniform wall temperature.  
Univ. of California, Inst. Eng. Research, Series, 2, No. 10, 1950.
20. Hartnett, J. P. ,  
Eckert, E. R. G. ,  
Birkebak, R. ,  
Sampson, R. L. Simplified procedures for the calculation of heat transfer to surfaces with non-uniform temperatures.  
WADC TR 56-373, 1956,
21. Baxter, D. C. ,  
Reynolds, W. C. Fundamental solutions for heat transfer from non-isothermal flat plates.  
J. Aero. Sci. , Vol. 25, 1958, pp 403-404.
22. Spalding, D. B. ,  
Pun, W. M. A review of methods for predicting heat-transfer coefficients for laminar uniform-property boundary layer flows.  
Int. J. Heat Mass Transfer, Vol. 5, 1962, pp 239-249.
23. Leveque, M. A. See Reference 6.
24. Klein, J. ,  
Tribus, M. Forced convection from non-isothermal surfaces.  
Eng. Res. Inst. , Univ. Michigan, 1952.

References (Continued)

25. Thwaites, B. Approximate calculation of the laminar boundary layer.  
Aero. Quarterly, Vol.1, 1949-1950, pp 245-280.
26. Walz, A. Ein neuer Ansatz für das Geschwindigkeitsprofil der laminaren Reibungsschicht.  
Lilienthal Bericht 141, 8., 1941.
27. Eckert, E. R. G., Hartnett, J. P., Birkebæk, R. Simplified equations for calculating local and total heat flux to non-isothermal surfaces.  
J. Aero.Sc., Vol. 24, 1957, pp 549-551.
28. Johnson, D.S. Velocity, temperature and heat transfer measurements in a turbulent boundary layer downstream of a step-wise discontinuity in wall temperature.  
J. Appl. Mech., Vol. 24, March, 1957, pp 2-8.
29. Rubesin, M W. An analytical investigation of convective heat transfer from a flat plate having a stepwise discontinuous surface temperature.  
A. S. M. E. Paper No. 48-A-42 (preprint) 1948.
30. Owen, P. R., Ormerod, A. O. Evaporation from the surface of a body in an airstream (with particular reference to the chemical method of indicating boundary-layer transition).  
Royal Aircraft Establishment Report Aero. 2431, 1951.  
A. R. C., R. & M. 2875, 1951.
31. Edwards, A., Furber, B. N. The influence of free-stream turbulence on heat transfer by convection from an isolated region of a plane surface in parallel air flow.  
Proc. Inst. Mech. Engrs., Vol. 170, 1956, pp 941-954.
32. Deissler, R. G. Analysis of turbulent heat transfer, mass transfer and friction in smooth tubes at high Prandtl and Schmidt numbers. NACA Report 1210, 1955.
33. Kestin, J., Persen, L. N. The transfer of heat across a turbulent boundary layer at very high Prandtl numbers.  
Int. J. Heat Mass Transfer, Vol. 5, 1962, pp 355-371.
34. Smith, A. G., Shah, V. L. The calculation of wall and fluid temperatures for the incompressible turbulent boundary layer with arbitrary distribution of wall heat flux.  
Int. J. Heat Mass Transfer, Vol. 5, 1962, pp 1179-1189.
35. Smith, A. G., Shah, V. L. Heat transfer in the incompressible boundary layer on a flat plate with arbitrary heat flux.  
J. of Aero/Space Sciences, Vol. 28, 1961, pp 738-739.
36. Shah, V. L. Theoretical and experimental study of heat transfer in an axisymmetric laminar boundary layer.  
M.Sc.(Eng.), Thesis, Univ. of London, 1961.
37. Shah, V. L. Heat transfer through an incompressible laminar boundary layer.  
College of Aeronautics Note 130, 1962.

# LIST OF SYMBOLS

$D$	diameter of the pipe, ft.
$x$	distance parallel to the wall and from the beginning of the boundary layer, ft.
$a$	distance where the heating starts, ft.
$y$	distance normal to the wall, ft.
$\xi$	variable of integration
$\psi$	stream function
$\delta$	boundary layer thickness, ft.
$\delta_2$	momentum thickness, ft.
$\delta_4$	shear thickness, ft.
$\Delta$	thermal boundary layer thickness, ft.
$\Delta_2$	enthalpy flux thickness, ft.
$\Delta_4$	heat flux thickness, ft.
$u$	velocity in the boundary layer, ft./sec.
$\bar{u}$	mean velocity parallel to wall in the pipe, ft./sec.
$u_1$	main stream velocity parallel to wall, ft./sec.
$V$	velocity normal to the wall, ft./sec.
$T$	temperature in the boundary layer, °F.
$T_1$	main stream temperature, °F.
$T_w$	temperature of the surface, °F.
$C$	concentration of the injected gas in the boundary layer in cu.ft./cu.ft.
$C_1$	concentration of the injected gas outside concentration boundary layer (this is zero) in cu.ft./cu.ft.
$C_w$	concentration of the injected gas at the surface in cu.ft./cu.ft.
$\mu$	viscosity, lb./ft.sec.
$\nu$	kinematic viscosity, ft <sup>2</sup> /sec.

### List of Symbols (Continued)

$\epsilon$	eddy viscosity, $\text{ft}^2/\text{sec}$ .
$h$	heat transfer coefficient $\text{BTU}/\text{sec}.\text{ft}^2. ^\circ\text{F}$ .
$k$	thermal conductivity $\text{BTU}/\text{sec}.\text{ft}. ^\circ\text{F}$ .
$h_c$	mass transfer coefficient $\text{cu}.\text{ft}./\text{sec}.\text{ft}^2$ .
$\rho$	density, $\text{lb}./\text{ft}^3$ .
$C_p$	specific heat $\text{BTU}/\text{lb} ^\circ\text{F}$
$D'$	diffusion coefficient, $\text{ft}^2/\text{sec}$ .
$\epsilon_h$	eddy thermal diffusivity $\text{ft}^2/\text{sec}$ .
$\epsilon_c$	eddy mass diffusivity $\text{ft}^2/\text{sec}$ .
$\alpha$	thermal diffusivity, $K/\rho C_p$ , $\text{ft}^2/\text{sec}$ .
$\tau_w$	shear stress at the surface, $\text{lb}./\text{ft}^3/\text{sec}^2$ .
$\dot{q}_w''$	heat transfer rate at the wall per unit area and unit time
$\dot{m}_w''$	mass transfer rate at the wall in $\text{lb}./\text{ft}^2/\text{sec}$ .
$u_\tau$	friction velocity $\sqrt{\tau_w/\rho}$
$r$	$= \left[ 1 - (a/x)^{3/4} \right]$
$s$	$= \left[ 1 - (a/x)^{9/10} \right]$
$I_{r(\alpha',\beta)}$	$= \frac{B_r(\alpha',\beta)}{B_1(\alpha',\beta)}$
$B_{r(\alpha',\beta)}$	$= \int_0^r \sigma^{(\alpha'-1)} (1-\sigma)^{(\beta-1)} d\sigma$

### Dimensionless

$\frac{\dot{q}_w''}{\rho C_p u_1 \sqrt{C_f}/2}$	= heat flux parameter
$u^+$	dimensionless velocity in boundary layer , defined by eq. 4.5
$x^+$	distance along the wall, defined by eq. 4.3
$x_{a,b}^+$	distance between points $x = a$ and $x = b$ , defined by eq. 4.27

# List of Symbols (Continued)

$y^+$	distance normal to the wall, defined by eq. 4.4
$\alpha^+$	thermal diffusivity, defined by eq. 4.7
$\epsilon^+$	eddy viscosity, defined by eq. 4.6
$\theta$	$= \frac{T - T_1}{T_w - T_1}$
$\theta_{a,b,c}$	value of $\theta$ at point C for constant heat flux parameter between $x = a$ and $x = b$
$\xi$	distance from the wall, defined by eq. 4.8
$Pr$	Prandtl number
$Sc$	Schmidt number
$Nu$	Nusselt number $\frac{hx}{K}$
$Re_x$	Reynolds number $\frac{u_1 x}{\nu}$
$Re_D$	Reynolds number $\frac{\bar{u}D}{\nu}$
$St$	Stanton number $\frac{h}{\rho u_1 C_p}$
$\frac{St}{\sqrt{C_f/2}}$	Spalding function
$C_f/2$	friction factor $\frac{\tau_w}{\rho u_1^2}$
	for pipe flow $\frac{\tau_w}{\rho \bar{u}^2}$

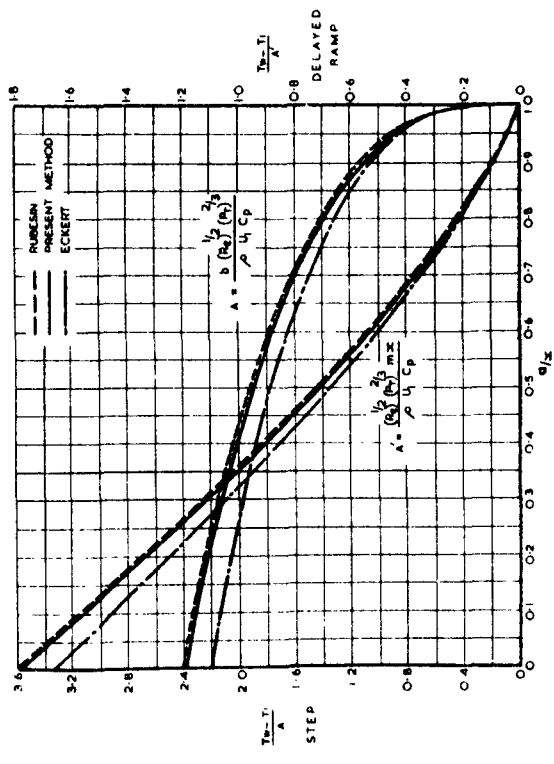


FIG 3.3 STEP AND DELAYED RAMP HEAT INPUT (LAMINAR BOUNDARY LAYER)

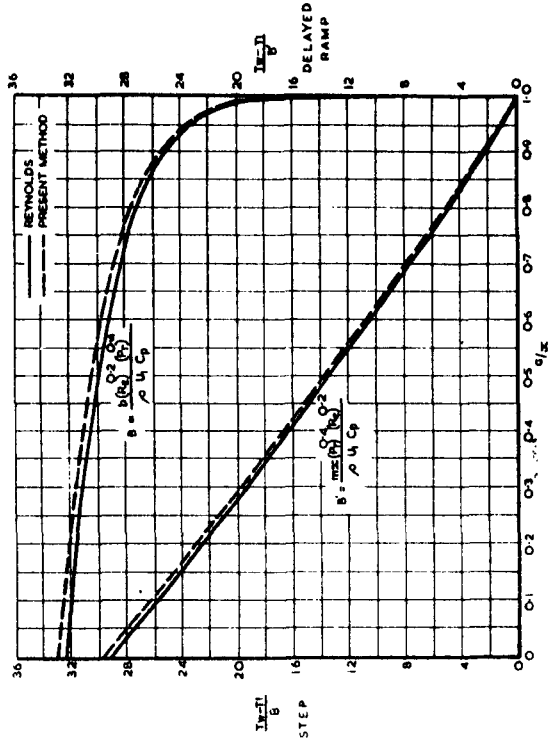


FIG 3.4 STEP AND DELAYED RAMP HEAT INPUT (TURBULENT BOUNDARY LAYER)

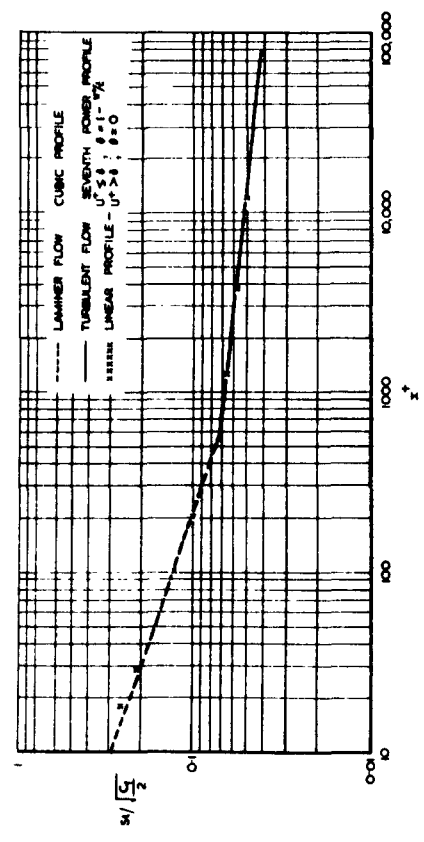


FIG 3.5 SPALDING FUNCTION ( $\theta^* = 1$ ) OBTAINED BY SOLVING THE INTEGRAL ENERGY EQUATION

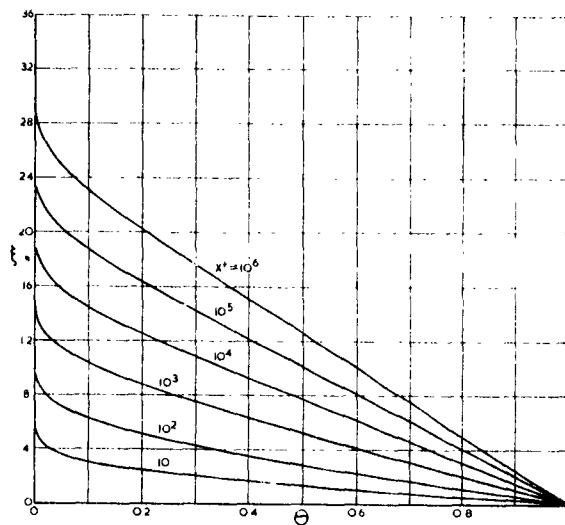


Fig 4.1 Temperature profiles for  $Pr=0.7$

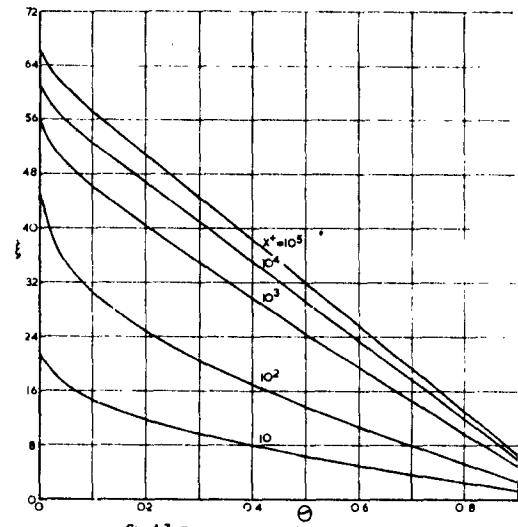


Fig 4.3 Temperature profiles for  $Pr=7$

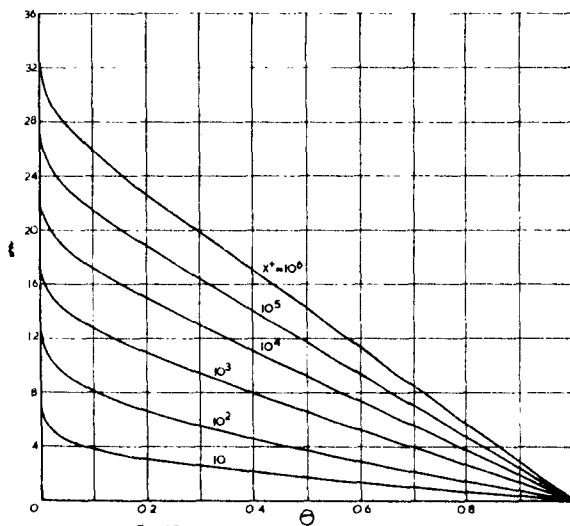


Fig 4.2 temperature profiles for  $Pr=1$

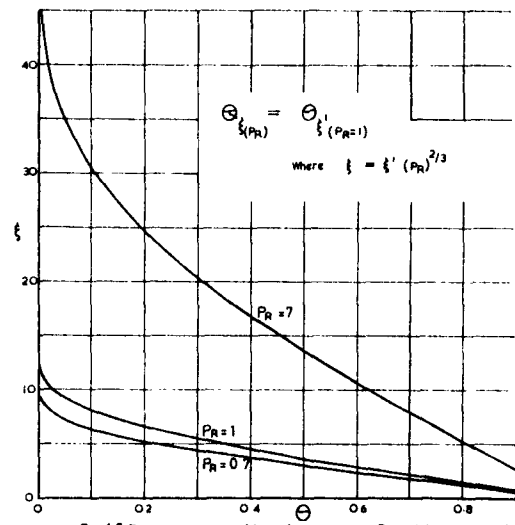


Fig.4.5 Temperature profiles for various Prandtl numbers ( $x'$  (Laminar region))

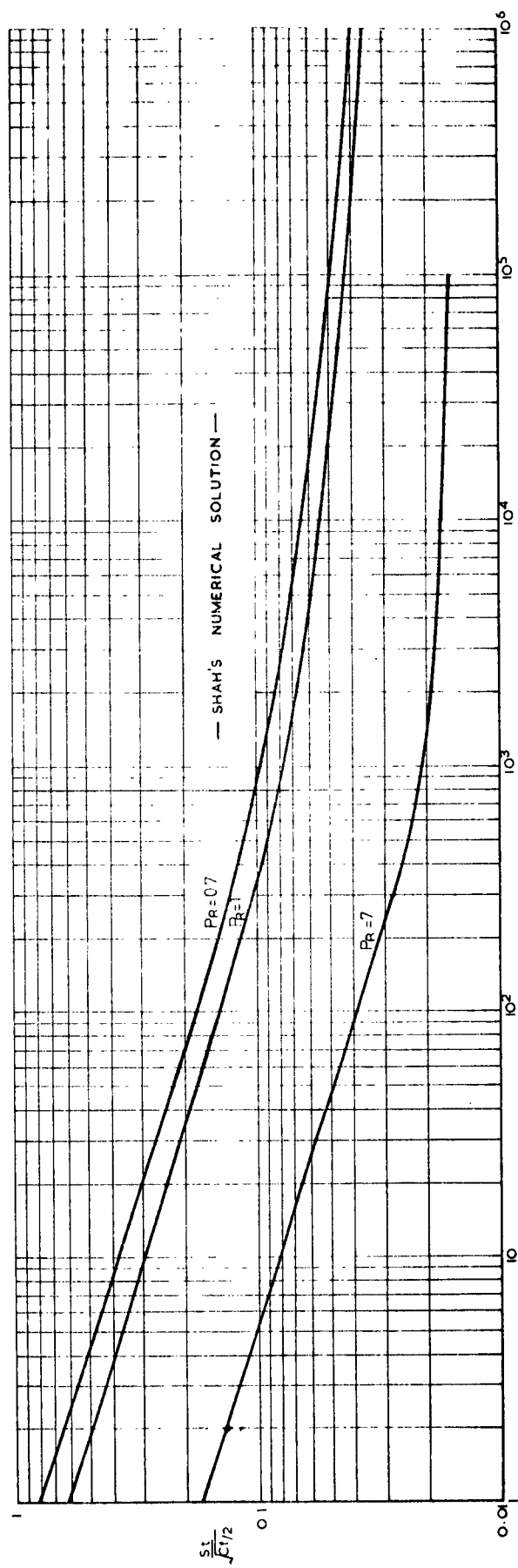


Fig.4.4 The Spalding Function  $\frac{S_1}{\sqrt{C_{1/2}}}(X^*)$  for  $Pr = 0.7, 1$  and  $7$

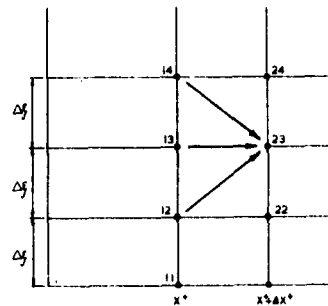
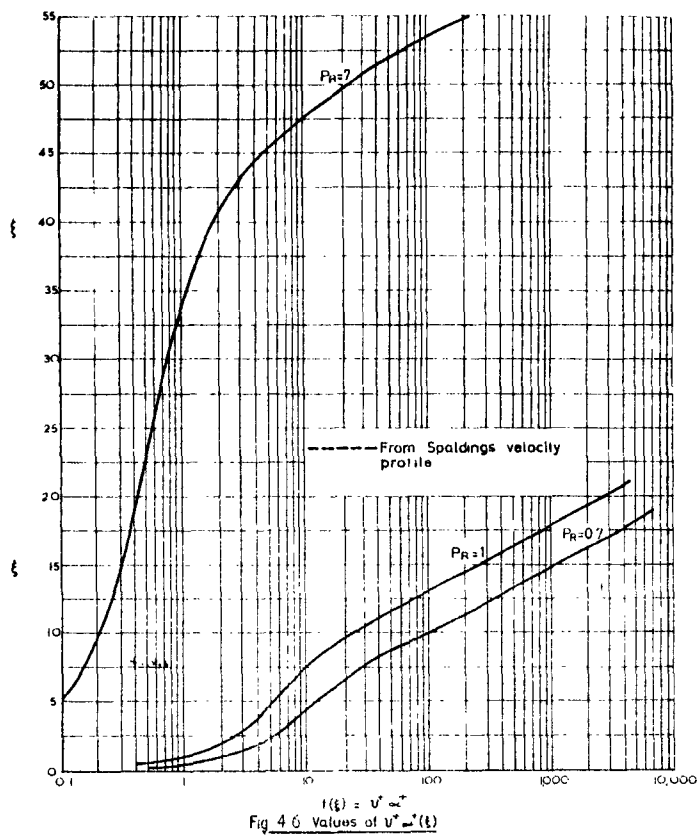
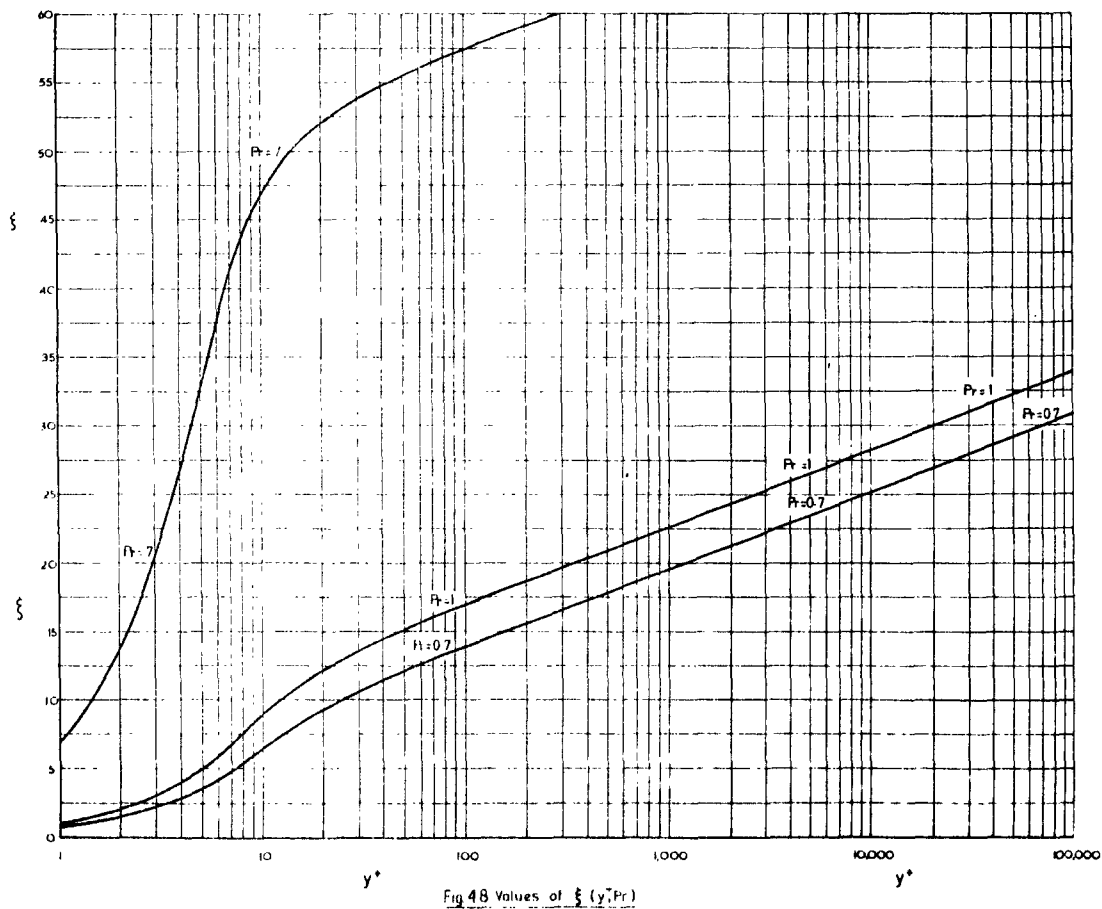
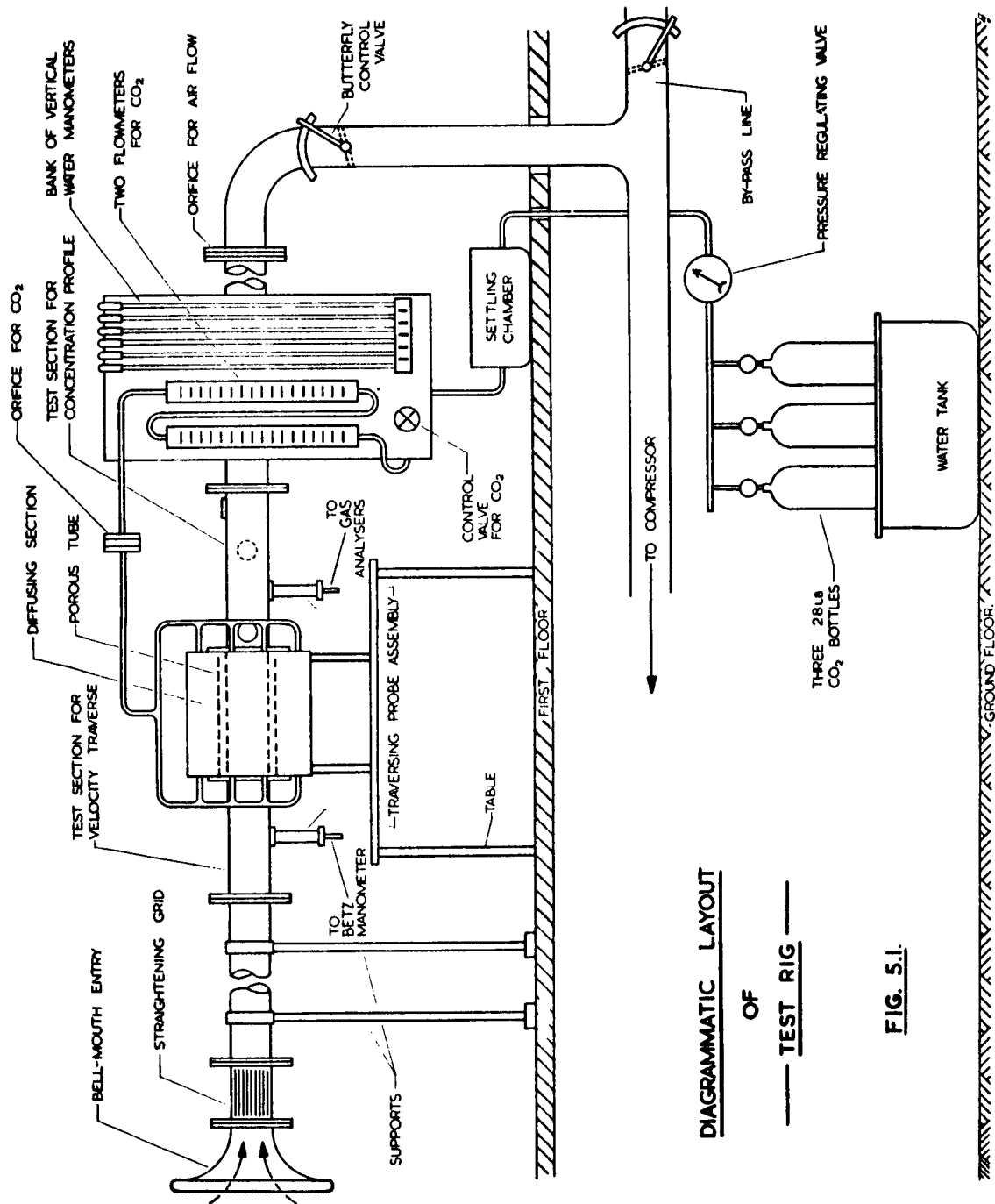


Fig 4.7 Grid for the finite difference scheme





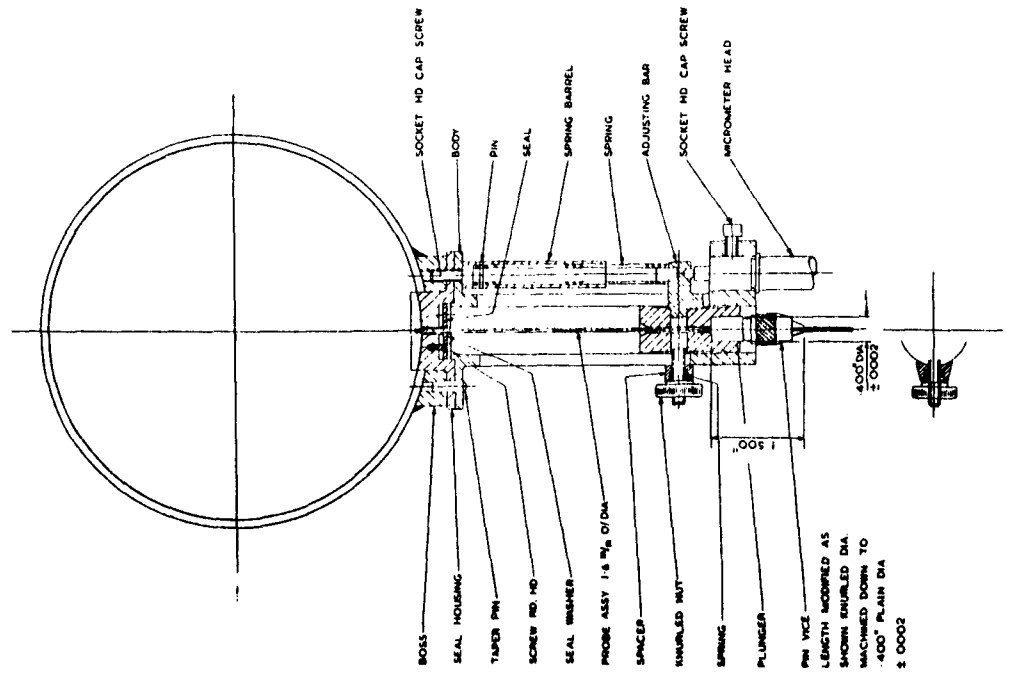


FIG. 52 TRAVERSING PROBE

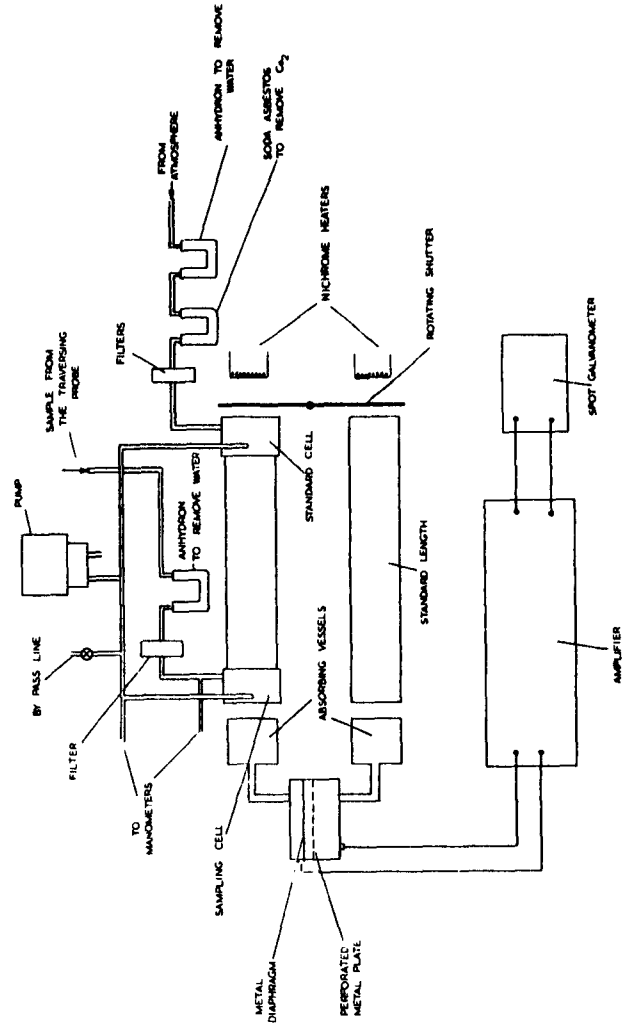


FIG. 5.3 LAYOUT FOR MEASURING THE CONCENTRATION OF CO<sub>2</sub>

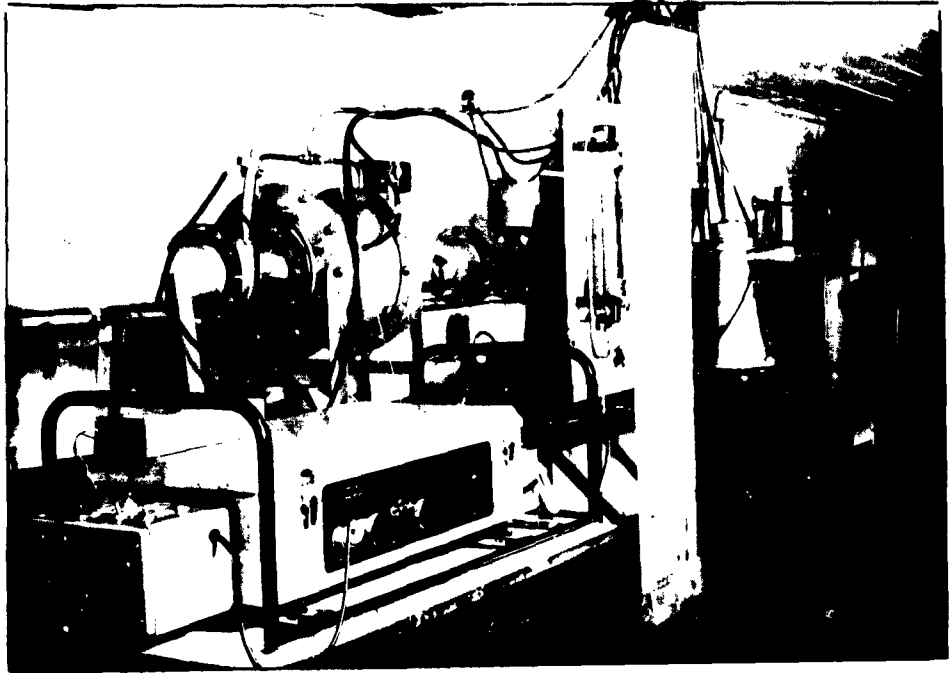


FIG. 5.4. TEST RIG

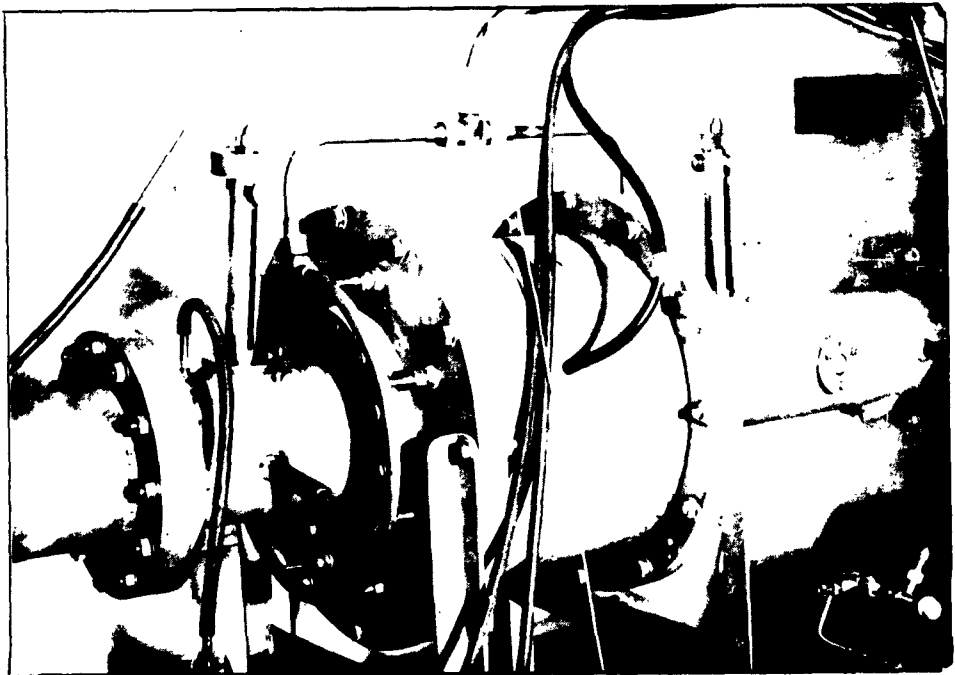


FIG. 5.5. CLOSE VIEW OF THE TEST SECTION

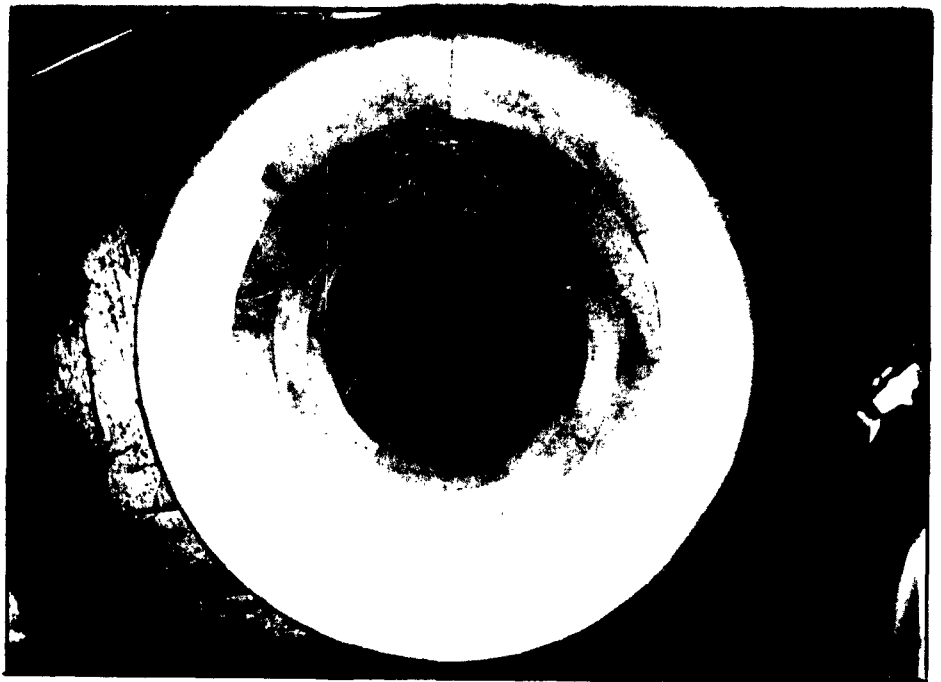


FIG. 5.6. BELL MOUTH ENTRY WITH STRAIGHTENING GRID

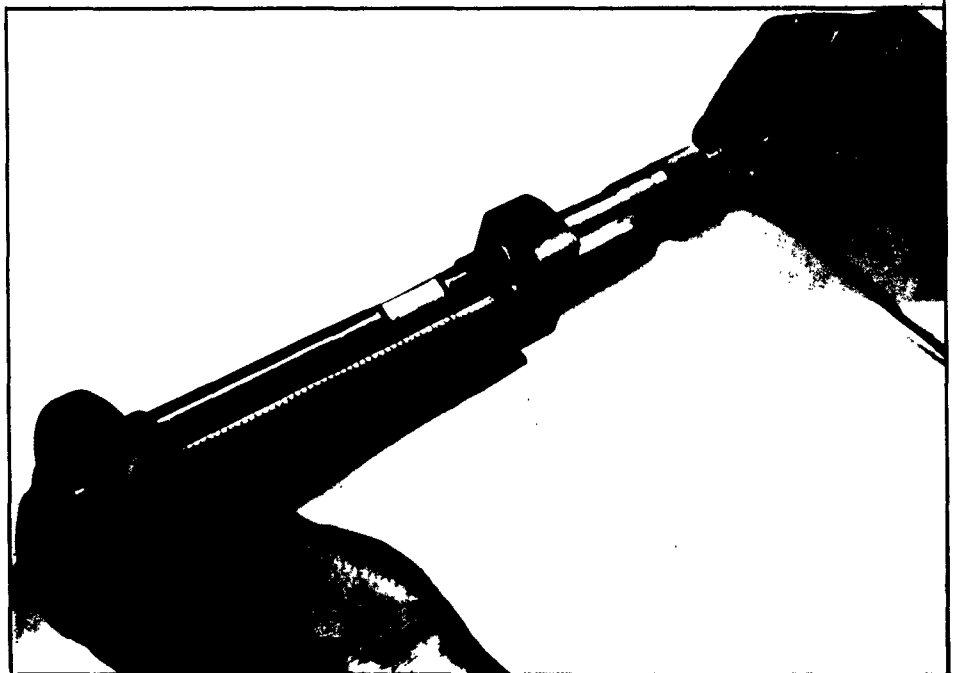


FIG. 5.7. TRAVERSING PROBE

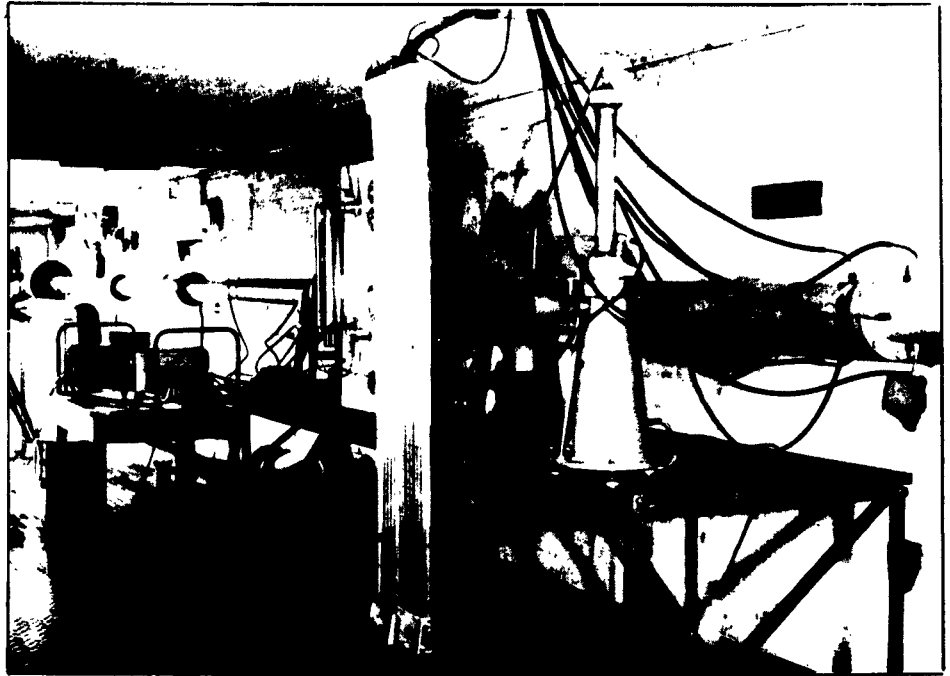


FIG. 5.8. TEST RIG

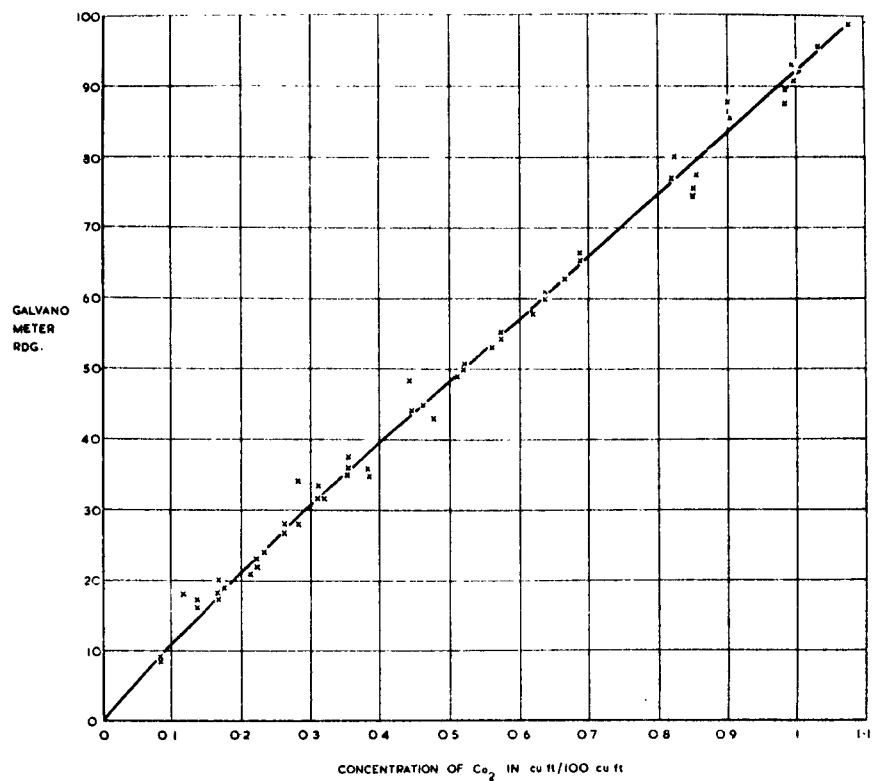


FIG.7.1. CALIBRATION OF THE INFRA RED GAS ANALYSER-RANGE 0-1.1 %.

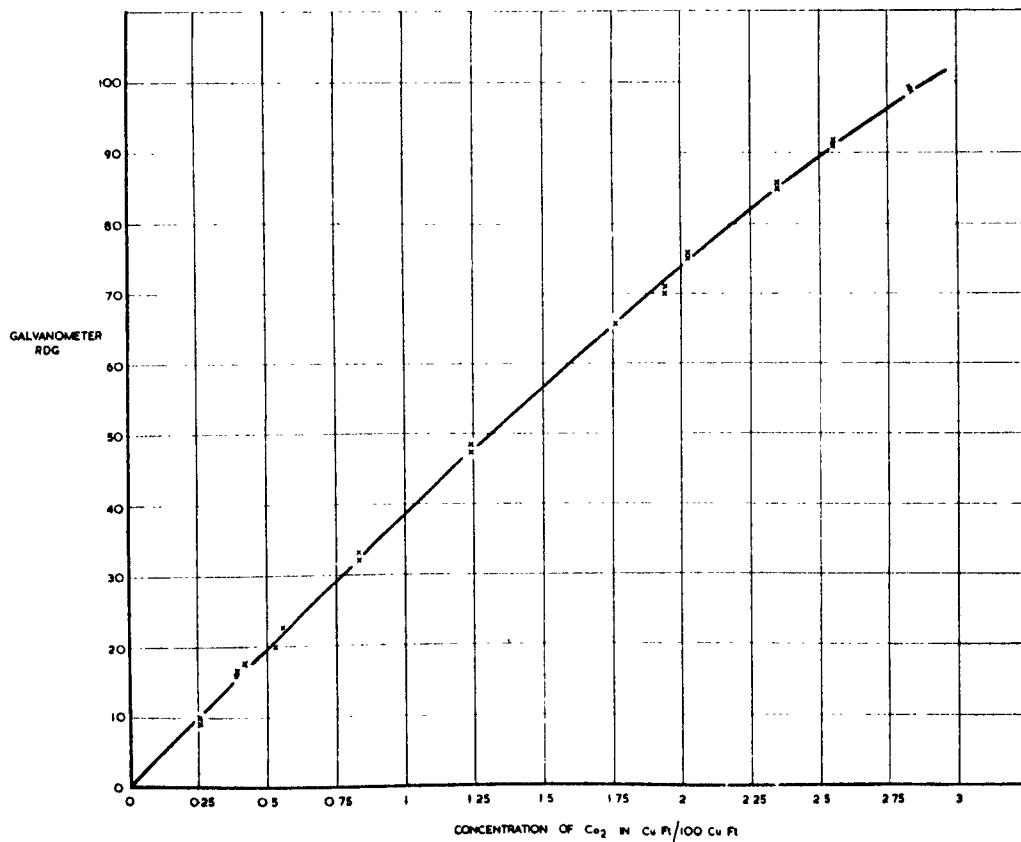


FIG. 7.2 CALIBRATION OF THE INFRA-RED GAS ANALYSER - RANGE 0-2.9%

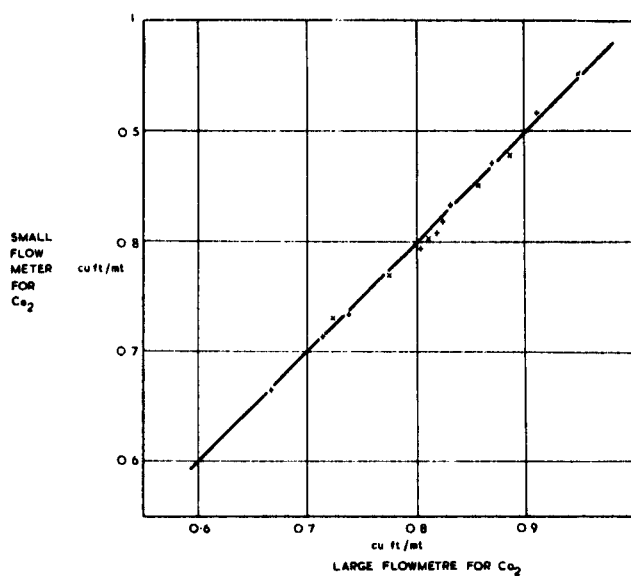


FIG. 7.3. COMPARISON  $\text{CO}_2$  FLOWMETER.

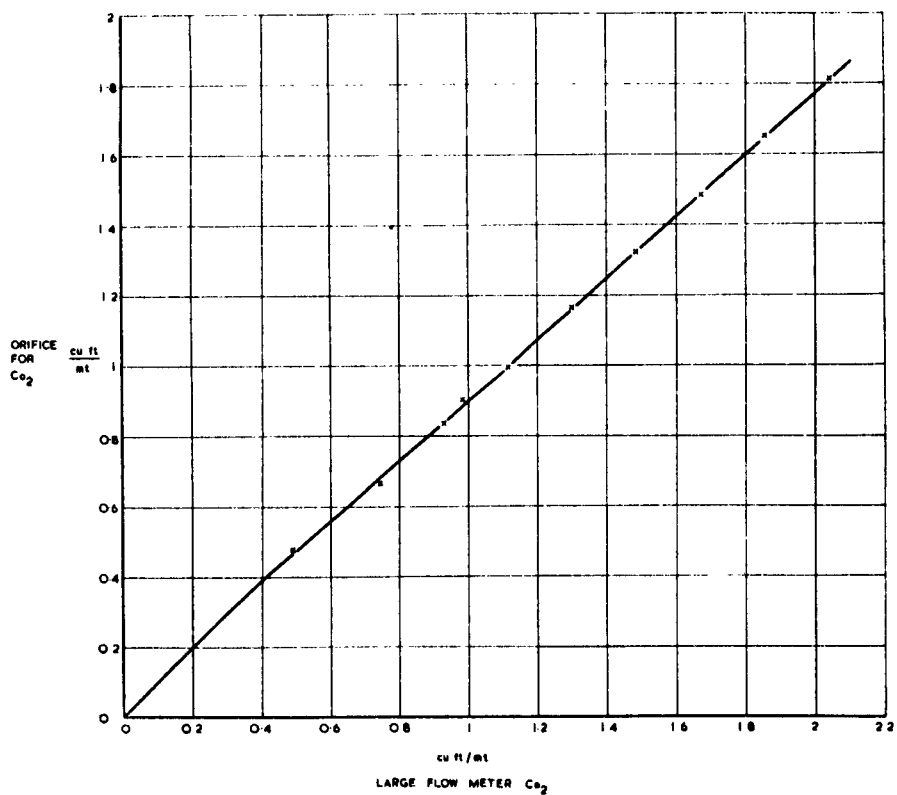


FIG. 7.4. COMPARISON OF  $\text{CO}_2$  FLOWMETER WITH ORIFICE.

$V^* = \text{FRICTION VELOCITY} = U_\tau \quad \nu = \text{KINEMATIC VISCOSITY.}$

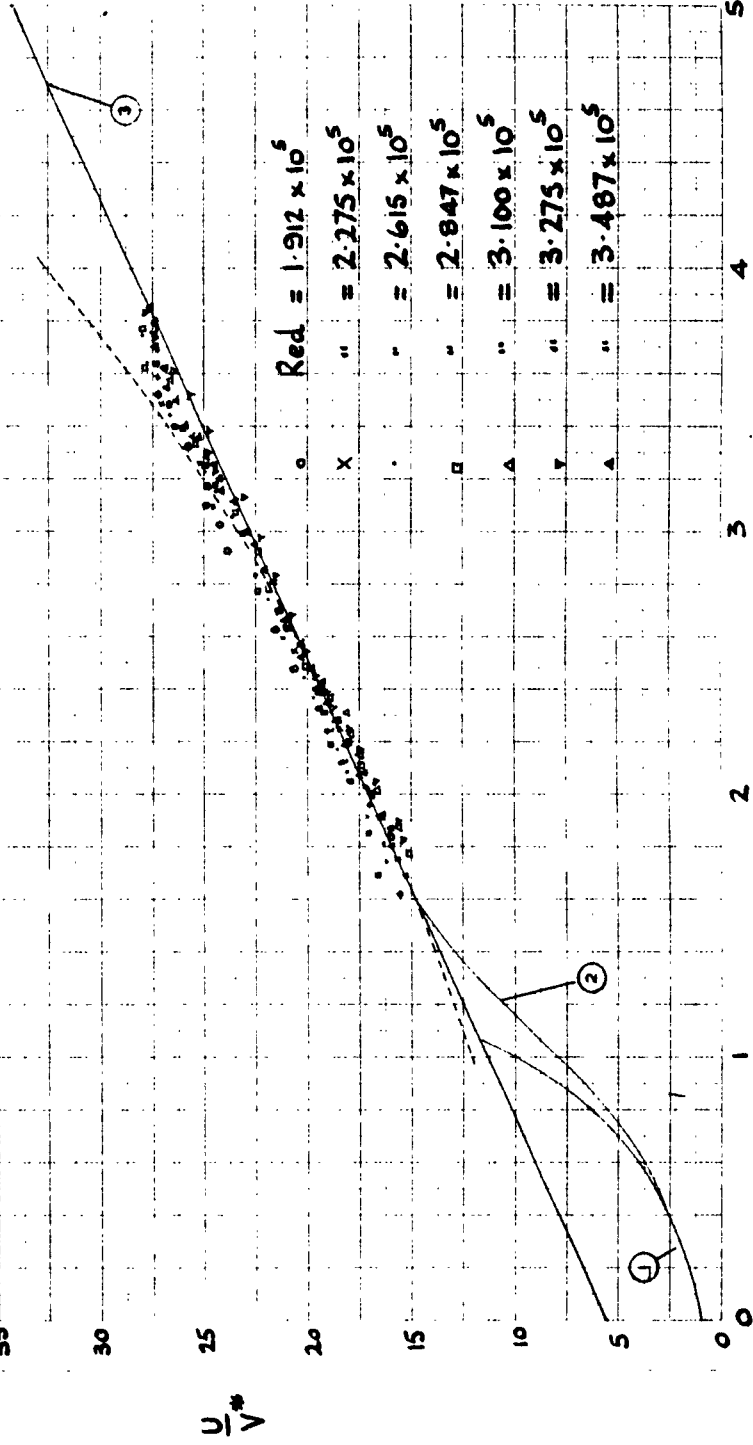
— UNIVERSAL LOGARITHMIC VELOCITY PROFILE

--- SEVENTH POWER PROFILE,

(1) LAMINAR SUBLAYER

(2) BUFFER LAYER

(3) TURBULENT REGION



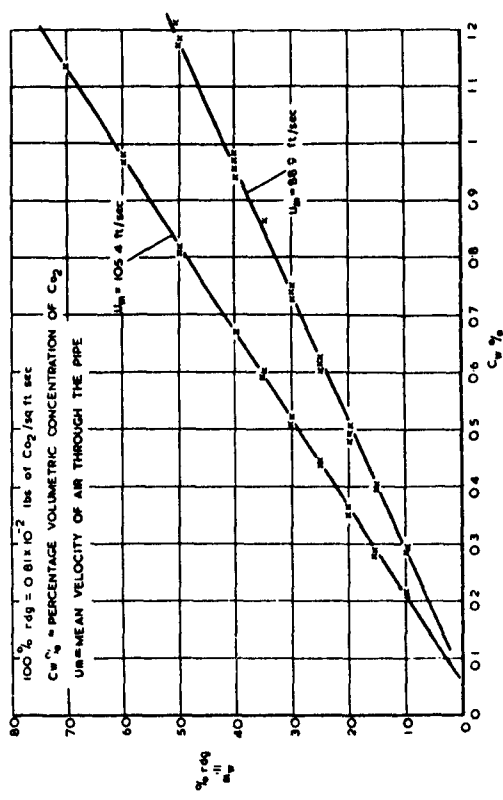


FIG. 7.7. VARIATION OF CONCENTRATION WITH THE INJECTION RATE

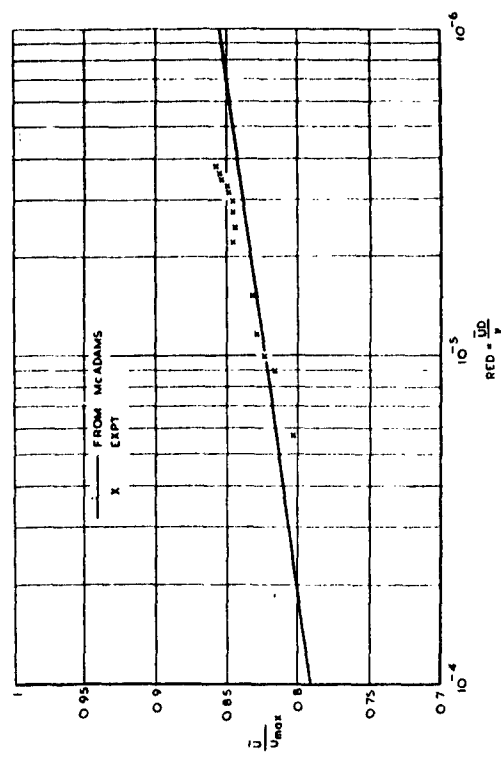


FIG. 7.8. RATIO OF THE AVERAGE VELOCITY TO THE MAX VELOCITY.

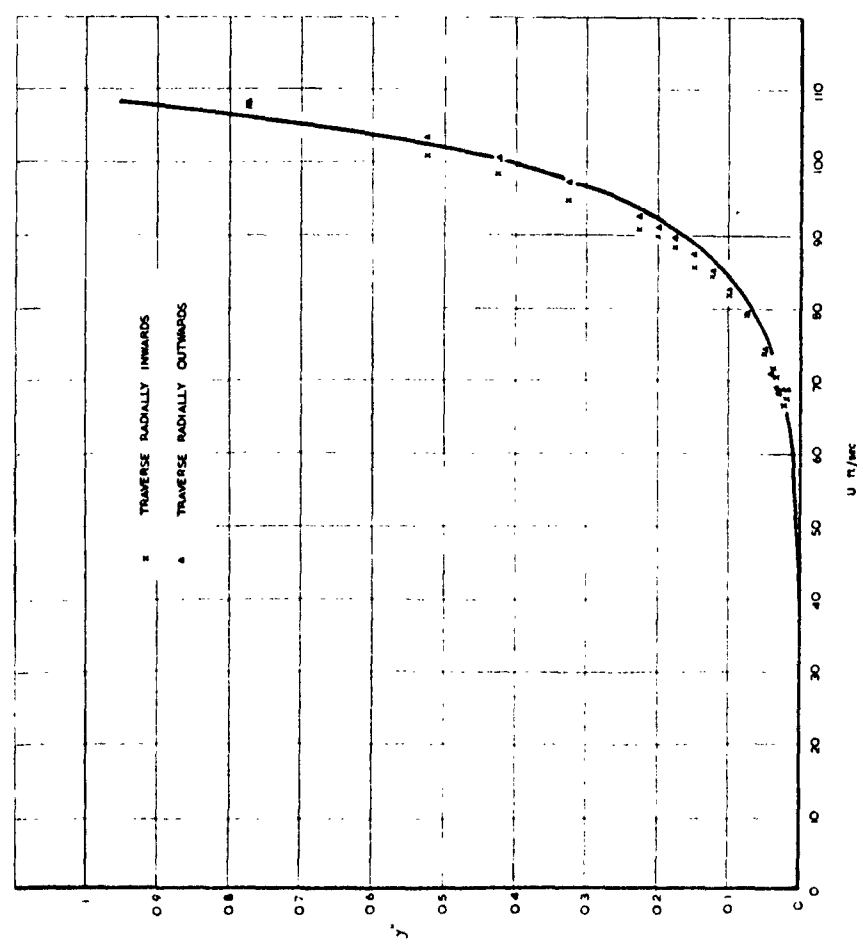


FIG. 7.6 COMPARISON OF EXPERIMENTAL VELOCITY PROFILE WITH SPALDING'S VELOCITY PROFILE.

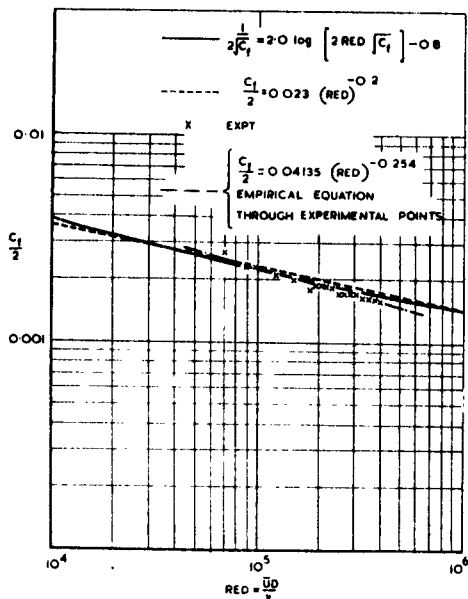


FIG. 7.9. MEASUREMENTS OF THE FRICTION FACTOR.

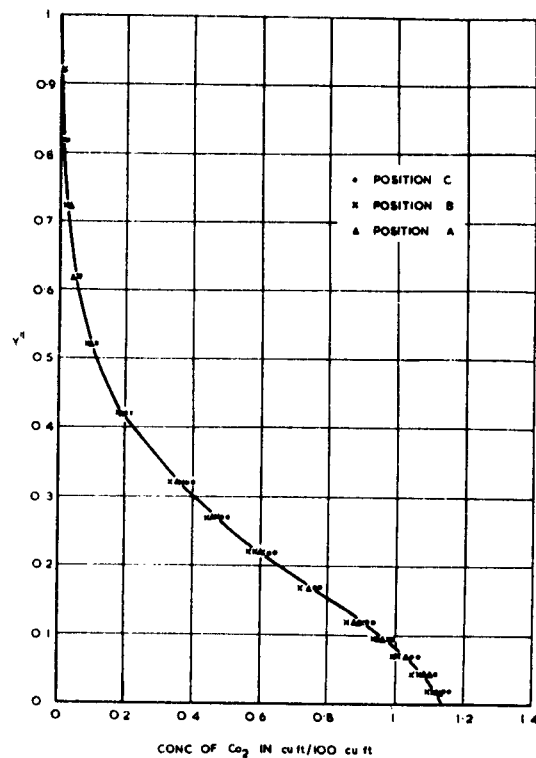


FIG. 7.11. THE CONCENTRATION PROFILE IN TEST I.

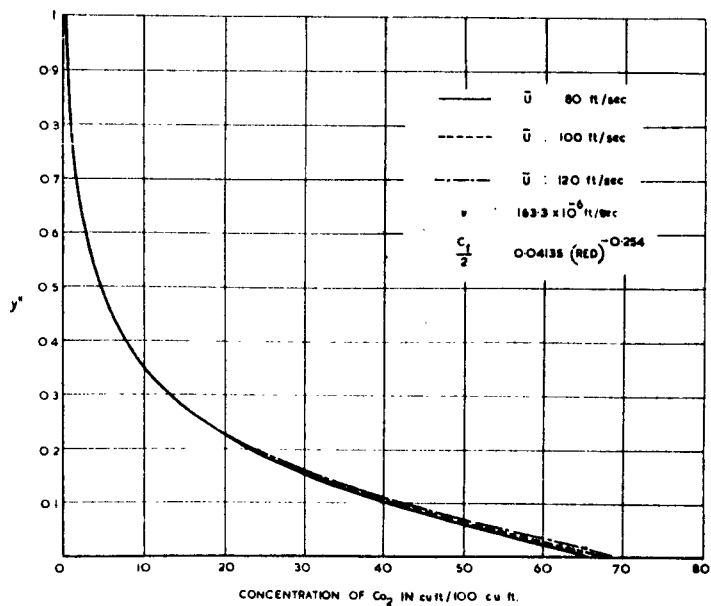


FIG. 7.10. THEORETICAL CONCENTRATION PROFILE AT SECTION I.

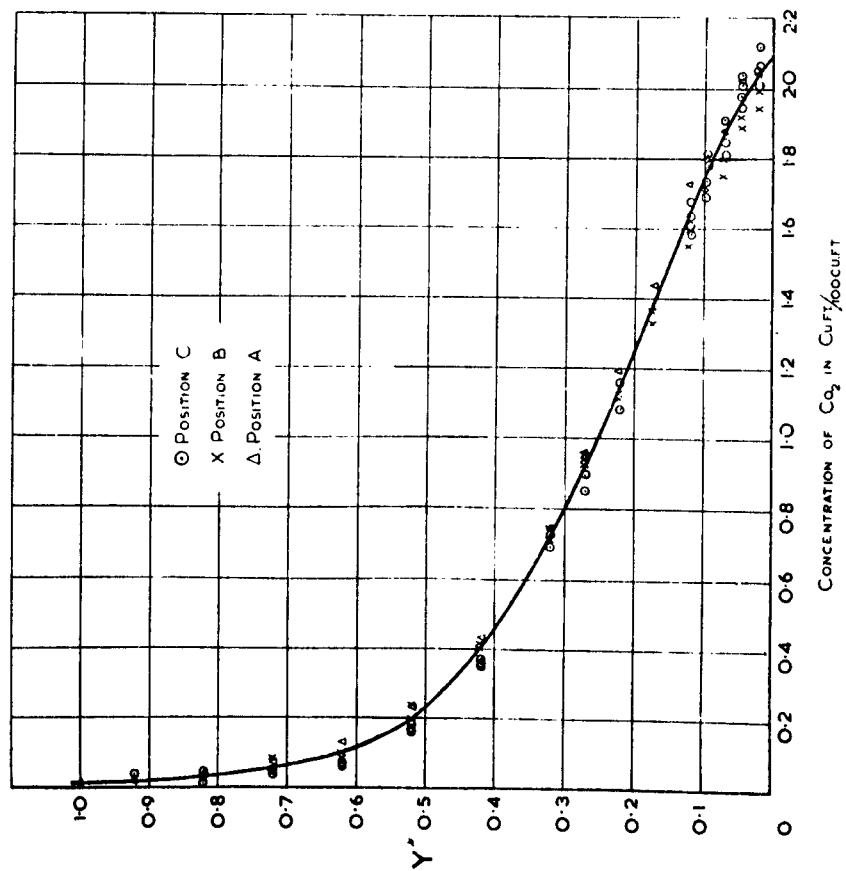


FIG. 7-12. THE CONCENTRATION PROFILE FOR TEST 2.

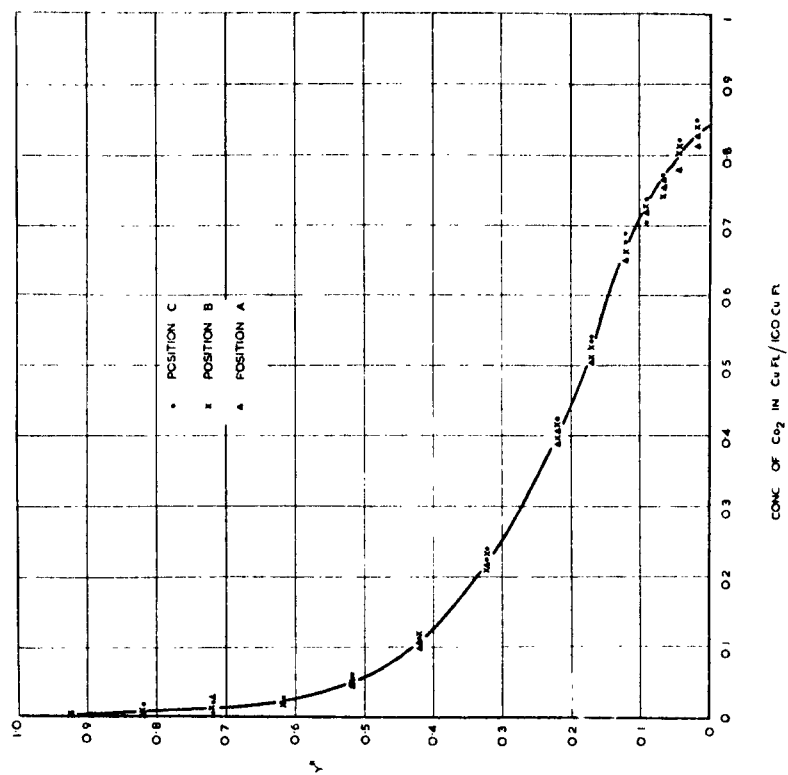


FIG. 7-13. THE CONCENTRATION PROFILE FOR TEST 3.

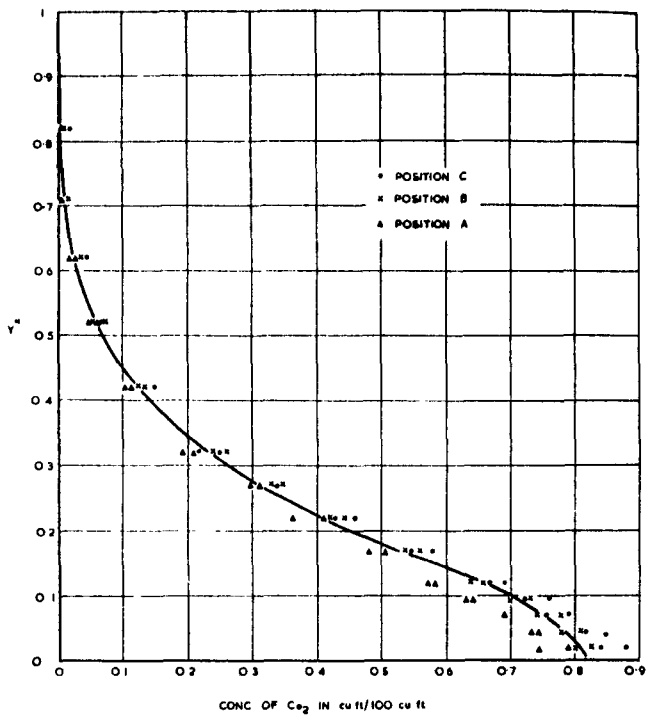


FIG. 7-14. THE CONCENTRATION PROFILE FOR TEST 4.

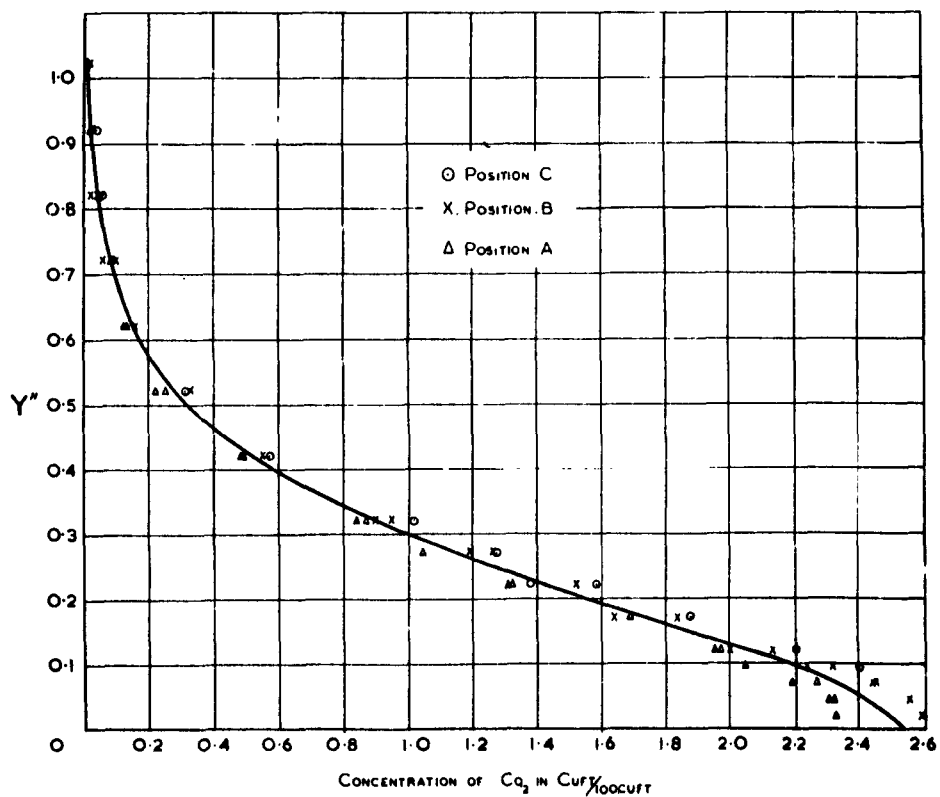


FIG. 7-15. THE CONCENTRATION PROFILE FOR TEST 5.

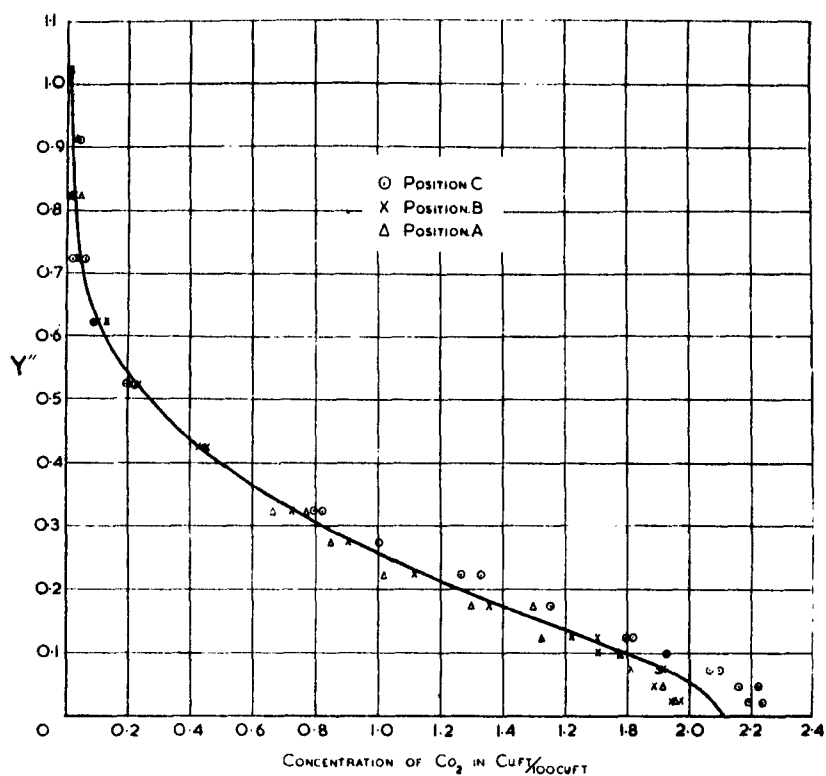


FIG. 7-16. THE CONCENTRATION PROFILE FOR TEST 6.

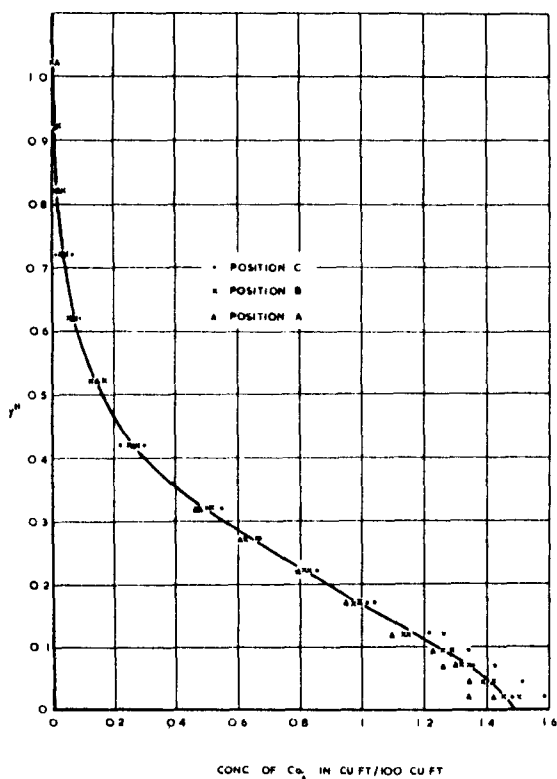


FIG 7-17. THE CONCENTRATION PROFILE FOR TEST 7

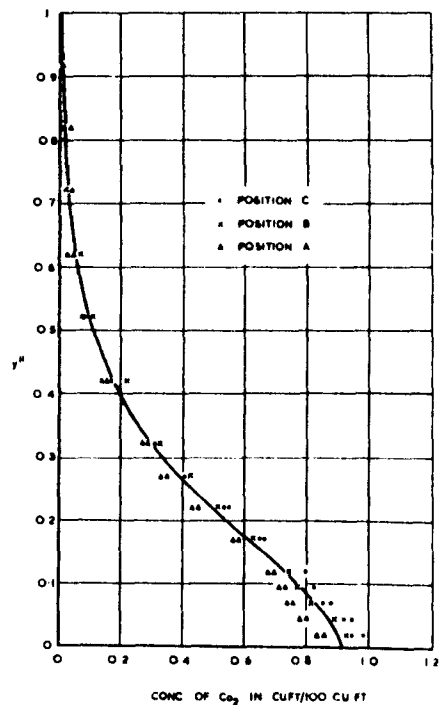


FIG. 7-18. THE CONCENTRATION PROFILE TEST 8.

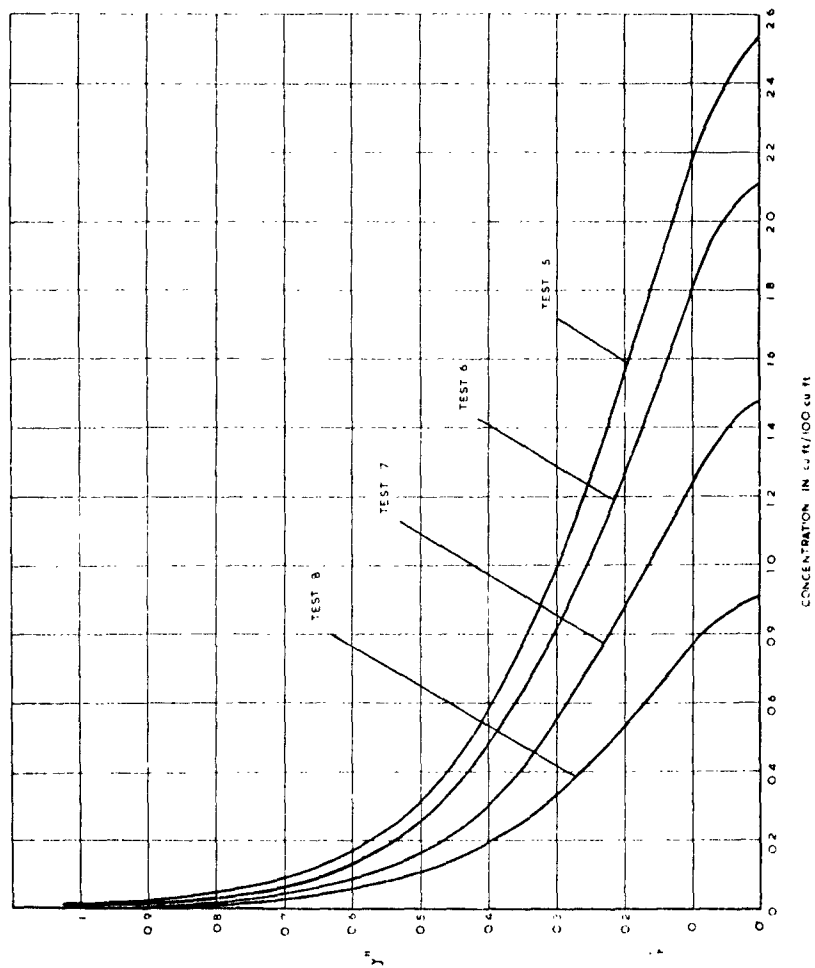


FIG. 7.19. VARIATION OF CONCENTRATION WITH THE INJECTION RATE.

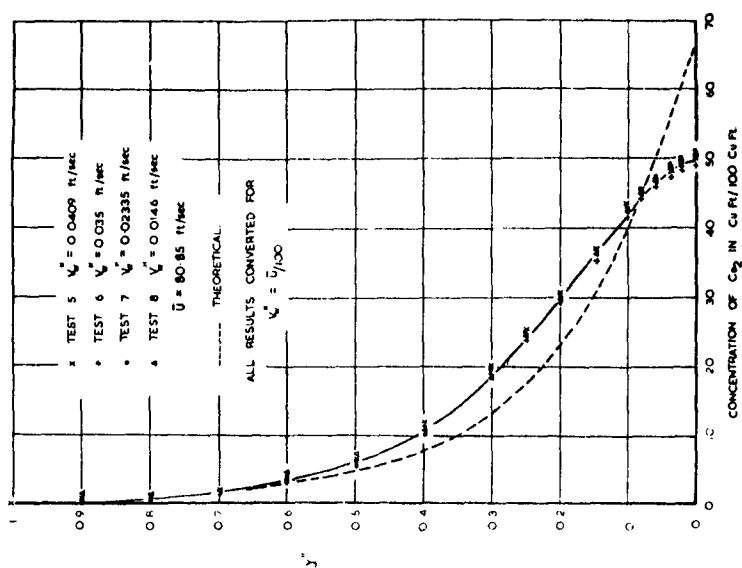


FIG. 7.20. COMPARISON WITH THEORETICAL SOLUTION

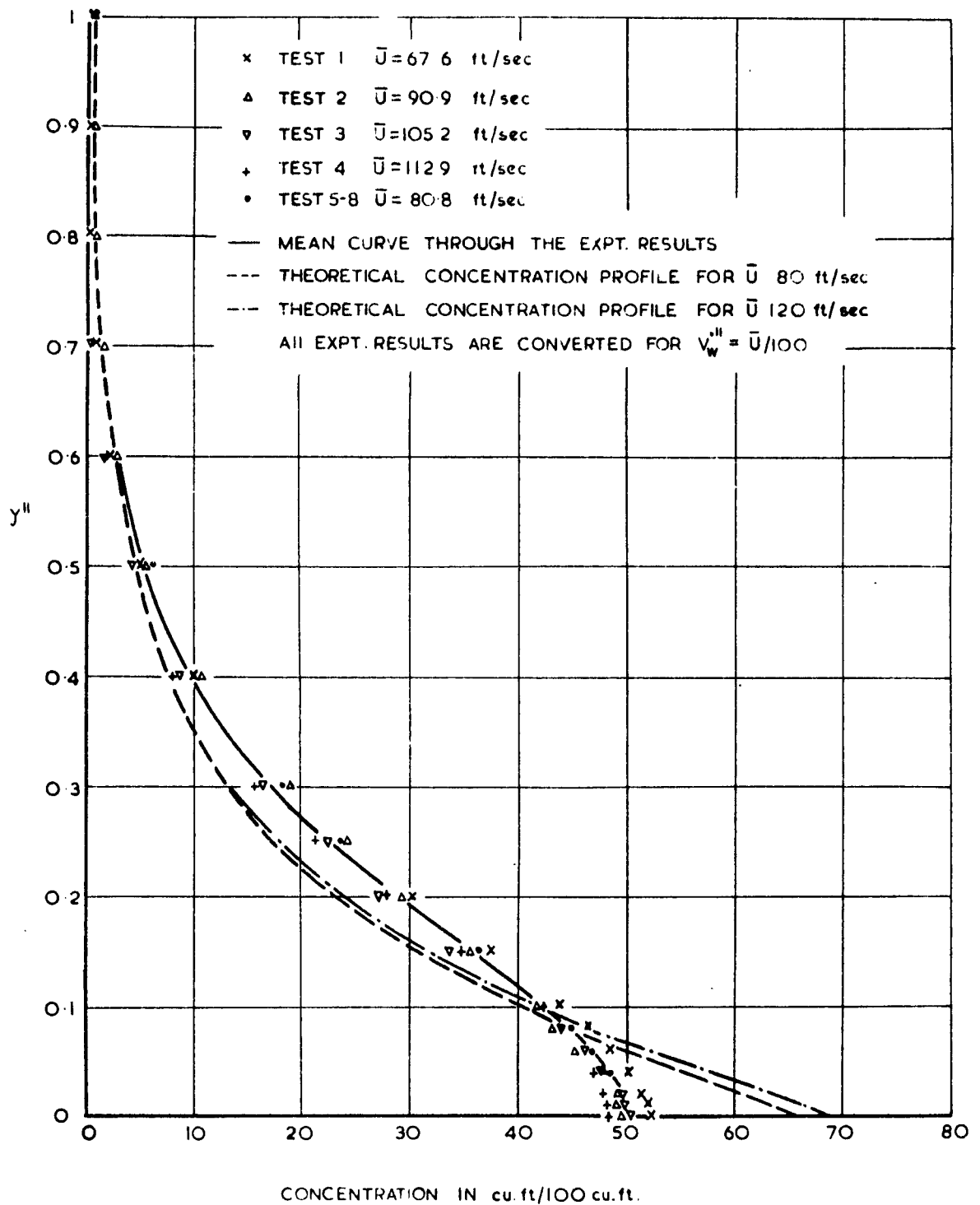


FIG. 7-21. COMPARISON WITH THE THEORETICAL SOLUTION.